FACE MORPHING ATTACK DETECTION IN THE PRESENCE OF POST-PROCESSED IMAGE SOURCES USING AVERAGING DIMENSIONALITY REDUCTION AND FEATURE-LEVEL FUSION

BY

KENNETH, Mary Ogbuka
M.Tech/SICT/2018/8479

DEPARTMENT OF COMPUTER SCIENCE
FEDERAL UNIVERSITY OF TECHNOLOGY, MINNA

AUGUST, 2021

FACE MORPHING ATTACK DETECTION IN THE PRESENCE OF POST-PROCESSED IMAGE SOURCES USING AVERAGING DIMENSIONALITY REDUCTION AND FEATURE-LEVEL FUSION

BY

KENNETH, Mary Ogbuka
M.Tech/SICT/2018/8479

A THESIS SUBMITTED TO THE POSTGRADUATE SCHOOL FEDERAL UNIVERSITY OF TECHNOLOGY, MINNA, NIGERIA IN PARTIAL FULFILLMENT OF THE REQUIREMENTS FOR THE AWARD OF THE DEGREE OF MASTER OF TECHNOLOGY IN COMPUTER SCIENCE

AUGUST, 2021

ABSTRACT

Face Morphing Attack Detection (MAD) has recently received a lot of attention because criminals have started to merge two or more subject facial images using publicly and widely obtainable digital manipulation techniques to develop a new facial image that can be interpreted as an accurate image of any of the individual images that make it up. Some of these tools generate high quality morphed images that pose a significant challenge to existing Face Recognition Systems (FRS). FRS has been shown to be vulnerable to multiform morphing attacks in the literature.Several forms of research on the detection of this morph attack have been carried out on the basis of this vulnerability using several techniques. Despite the high levels of MAD recorded in the literature, no suitable solution for handling post-processed pictures, such as those updated after morphing with a sharpening operation that significantly reduces visible artefacts in morphed photos, has yet to be discovered. In this work, before image post-processing and after image post-processing, an approach is proposed for MAD based on averaging dimensionality reduction and feature-level fusion and classification using Support Vector Machine (SVM). The outcome of SVM training with fused feature vectors increased the accuracy of the classification from 94% to 97.1%, thus enhancing overall performance.

TABLE OF CONTENTS

LIST OF TABLES

LIST OF FIGURES

LIST OF PLATES

CHAPTER ONE

1.0 INTRODUCTION

1.1 Background to the Study

Biometrics is the process of automatically recognising individuals based on their biological and behavioral characteristics (Scherhag *et al*., 2017). Biometric systems are becoming more common as a result of the clear connection between subjects and their biometric characteristics, as well as the user convenience (Tolosana *et al*., 2020). Biometric characteristics are so unique to an individual that they can be used for authentication, access control, and identification for example in smartphone unlocking, border control, national identity card, driving license, forensic identification, and voter's card (Kramer *et al*., 2019). Biometric features such as fingerprints, iris, voice, and facial characteristics are used for authentication and identification. One huge advantage and a reason for biometric verification success is that every individual carries his or her biometric characteristics always with them and these characteristics are also difficult to copy or duplicate by another individual (Seibold *et al*., 2018). Face as a biometric method is an recognized means for verification of individual identity because of the continuous knowledge of the capture process and the customer convenience involved (Deshpande & Ravishankar, 2017). A printed face image has been an integral part of identity documents for many years. Digital face images stored on a chip embedded in the document have increasingly been used to replace printed face images. On the one side, distributing machine-readable documents with digital images opens up new possibilities for using automatic facial recognition systems for identity authentication, saving money and time (Makrushin *et al*., 2017). Face Recognition Systems (FRS) deals with automatic recognition of individuals by observing their facial characteristics (Raghavendra *et al*., 2016). FRS are based on information gathered over the last 40 years from pattern and

signal recognition systems, resulting in accurate and dependable FRS. Face biometrics are now being used in various applications, including forensics, criminal identification in airports and train stations, surveillance, credit card authentication, logical and physical access control to e-Government applications. Biometric facial reference images have become an important portion of e-passports (Damer *et al*., 2018a), which has now achieved a distribution of close to 800 million passport instances after a 10 years introduction cycle. Thus face recognition using these passports is now a prominent application in border control setting (Ferrara *et al*., 2014). Face recognition is used for the border control situation because, in the event of an incorrect device decision, the border control officer would perform a visual comparison, which is a unique benefit over other biometric models such as fingerprint recognition (Mislav *et al*., 2021). These factors justify the usage of FRS in Automatic Border Control (ABC) e-gates (Raghavendra *et al*., 2016). The relation between both the electronic Machine Readable Travel Document (eMRTD) and the passport owner (the person who presents the eMRTD to the border officer) is spontaneously checked in an ABC system by matching the live-captured face picture with the facial reference photo stored in the eMRTD passport. This has increased the value of ABC systems, which are based on highly efficient and precise border control processes (Raghavendra *et al*., 2016).

With the wide acceptance of ABC systems, the susceptibility of FRS, as a key technical component of an ABC system, to various types of attacks has gotten a lot of attention. These attacks can be divided into two categories. The first form of attack is on the ABC system itself, which is usually performed by introducing a face artefact to the capture unit. Face spoofing or presentation attacks are examples of this attack (Bharadwaj *et al*., 2013; Tolosana *et al*., 2020). However these attacks involve a great effort in producing a face artefact and also in submitting the same to the ABC e-gate. Besides that this types of

attack will only be effective, If an intruder can gain access to a misplaced eMRTD passport, the intruder would be able to create a face artefact that matches the eMRTD passport's face image (Chingovska *et al*., 2019). The second type of attack is an eMRTD biometric reference attack, in which biometric data encoded in the (illicit) passport's logical data structure is manipulated with the aim of replacing the reference image. This attack is easy to carry out since most passport applications allow a printed face picture as part of the application process. Additionally, many countries will receive digital photograph uploads to a web-application for passport renewal and VISA applications. This will give an intruder plenty of opportunities to apply a fictitious face picture to the passport delivering agency and obtain an genuine eMRTD passport with both electronic and physical security features and the fictitious photograph (Raghavendra *et al*., 2016).

To carry out an invasion on the eMRTD biometric reference picture, simple changes can be made using easily accessible software (Ferrara *et al*., 2016). Face morphing is becoming one of the most important assault on the ABC border control mechanism among the various types of face picture alterations (aspect ratio, geometric and beautification) (Debiasi *et al*., 2018a). Face morphing is a technique for creating a new face picture from the unique details contained in two or more source face photos belonging to two or more different individuals. As a result, the morphed face image would eventually represent the facial features of many data subjects who contributed to the morphed face. Any attacker can morph his face into that of another (defenseless) subject and request for an eMRTD passport that both subjects can use. This defective connection of multiple subjects with the document could result in a variety of illegal activities such as human trafficking, financial transaction, and illegal immigration (Damer *et al*., 2019).

Humans are unable to detect morphed facial images, as shown by by Ferrara *et al*. (2014), Damer *et al*. (2018a), Kramer *et al*. (2019) and Scherhag *et al*. (2019b). Given the

widespread use of eMRTD passports with ABC border control systems, any intruder can carry out this assault without ever falsifying a passport document. As a result, to ensure the reliability of border control processes, these types of attacks must be mitigated. In the study by Kramer *et al*. (2019) on Face Morphing Attack Detection (MAD) by computers and humans revealed that humans were greatly prone to errors when detecting morphs, and that training these humans had little impact. However experiment on MAD using computer showed to be more effective as it outperformed the human participants.

In the previous years, there have been few authors who have worked on MAD. In 2014 Ferrara *et al*. (2014) introduced face morphing attack which was called the magic passport. The viability of attacks on Automated Border Control (ABC) systems using morphed face images was examined. It was concluded that when the morphed passport is presented, the officer will recognise the photograph and release the document if the passport is not substantially dissimilar from the candidate's face. And thus, the released document passes all authenticity checks carried out at the gates.

Raghavendra *et al*. (2016) carried out novel research on how this face morphing attack can be detected. The study was conducted using facial micro-textures retrieved via statistically autonomous filters, which are trained on natural photographs. This micro-texture dissimilarity was extracted using Binarised Statistical Image Features (BSIF), and classification had been made via Support Vector Machine (SVM). This was the first research done towards the MAD. Later in 2017, Seibold *et al*. (2017) aimed to perform MAD using a deep neural network. Three Convolutional neural network architecture were trained from scratch and using already trained networks to initialise the weights. Pretrained networks were noticed to outperform the networks trained from scratch for each of the three architecture. Hence it has been concluded that the attributes acquired for classification tasks are also beneficial for MAD. In 2018 Wandzik *et al*.

(2018) suggested a method for MAD based on a general-purpose FRS. In this work, a general-purpose FRS was combined with a simple linear classifier to successfully detect morph images while Spreeuwers *et al*. (2018) created face morphing databases with varying characteristics and performed MAD on these various morphed images based on local binary pattern extracted features and classification was performed using support vector machine. To exam the system's robustness, an experiment was carried out on a mixed dataset generated with various morphing software and images with artefacts hidden by Gaussian noise.

In 2019 Venkatesh *et al*. (2019a) and Singh *et al*. (2019) developed MAD techniques. Venkatesh *et al*. (2019a) presented a novel approach for MAD focused on quantifying residual noise caused by the morphing phase. An aggregation of several denoising methods estimated using a deep Multi-Scale Context Aggregation Network (MSCAN) was used to quantify the morphing noise . Deep features were computed using a pre-trained AlexNet based on the residual noise from deep MSCAN. The Collaborative Representation Classifier (CRC) was trained using the features extracted to arrive at the final decision. When lighting, pose, and print-scan artefacts are present, Singh *et al*. (2019) used deep decomposed 3D structure and diffuse Reflectance to achieve MAD in the presence of pose, lighting and print-scan artefacts. To improve robustness and generality, Seibold *et al*. (2020) proposed neural network training strategies depending on distinct training data alternations. The layer-wise significance propagation method was used to investigate the gaps in the decision-making processes of the variously qualified neural networks. Peng *et al*. (2019) and Ortega-Delcampo *et al*. (2020) did not just stop at detecting face morphing attack but went further to de-morph the morphed face images. Peng *et al*. (2019) performed image de-morphing using the generative adversarial

network to rebuild the accomplice's facial image, and Ortega-Delcampo *et al*. (2020) used the CNN approach for morphed image de-morphing.

Studies conducted by Ramachandra *et al*. (2020), Jassim and Asaad (2018), Wandzik *et al*. (2018), and Seibold *et al*. (2018) have yielded excellent detection rates. These results, on the other hand, are only tangentially applicable to post-processed images, like image enhancement/sharpening and compression, that can significantly reduce observable morphing artefacts and make the earlier algorithms ineffective. As a result, even after the morphed images have been post-processed, it's important to detect this morphing attack seamlessly. In this study, MAD was conducted in the presence of sharpened image sources using averaging dimensionality reduction and summation feature level-fusion of gradient features..

1.2 Statement of the Research Problem

Since FRSs and humans have limited capacity to mismatch morphed photos, morphing detection is needed at both the implementation and use stages of a document for identity verification (Jassim & Asaad, 2018; Makrushin & Wolf, 2018). Furthermore, the resultant importance of detecting fake passports at the ABC gate is not in doubt. Nonetheless, one of the significant concern in MAD is detecting morphed images even after been processed or altered. After making the morphed face picture, for example, the image could be further manipulated and changed. By purposefully improving or reducing the image quality, the image distortion (morphing) could be concealed. The automated production of morphed face pictures, in particular, can result in morphing artefacts. Shadow or phantom artefacts may be caused by missing or misplaced landmarks. To fix the problems of the morphed face image, the facial area can be substituted with an adjusted outer space from one of the subjects. To conceal artefacts in the hair region, Weng *et al*. (2013) suggests an

interpolation of the hair region. Morphing artefacts in the hair region, on the other hand, may be obscured by interpolating the hair region (Weng *et al*., 2013).

However, irregular color gradients and edges can occur as a result of insufficient interpolation methods, which can be mitigated by sharpening or blurring. Because of the averaging performance during the merging phase, the color value histograms can become narrow. This morphing artefact can be made by adapting the color histogram to achieve realistic histogram shapes that can mask or minimize the morphing artefact, preventing MAD systems from detecting such morphed photos.

Another challenge encountered in MAD is the lack of a robust publicly available database. Since there are no vast publicly accessible databases of morphed and bona-fide databases, researchers had to create morphed images using morphing software in most MAD study (Makrushin & Wolf, 2018; Scherhag *et al*., 2019a). Some of the initially available databases do not exist anymore. Various in-house databases have been used to perform research. This challenge prevents creating functional and robust comparative benchmarks for existing MAD algorithms because of the different datasets and protocols. Hence, in line with these identified challenges, this research proposes a MAD system in the presence of post-processed (image sharpening) image sources based on averaging feature dimensionality reduction and summation feature-level fusion of 8x8 and 16x16 scale HOG gradient descriptor using SVM. In this project the created morphed image dataset, as well as the post-processed (sharpened) morphed image dataset, will be made publicly available for MAD. The dataset is built in such a way that it is free of prejudice.

1.3 Aim and Objectives

This study aims to detect face morphing attacks in the presence of post-processed image sources based on averaging dimensionality reduction and summation feature-level fusion of gradient features using SVM. The Objectives of this study are to:

i. Generate a morphed image dataset and post-processed morphed image dataset.

ii. Develop a dimensionality reduction and feature-level fusion technique.

iii. Evaluate the technique's performance in (ii) using False Acceptance Rate, False Acceptance Rate and Accuracy performance metric.

1.4 Scope of the Research

This study's primary focus is to detect face morphing attacks using only gradient features without considering texture, deep, image degradation, and keypoint features. The proposed system is based on averaging dimensionality reduction and summation feature level fusion. Principal component Analysis (PCA) and Neighbourhood components analysis were not considered for dimensionality reduction. Morphed image de-morphing was also not considered.

1.5 Significance of the Study

The importance of this research effort in addressing the challenge of MAD in the presence sharpened mage sources cannot be exaggerated. The need for such innovation has a positive impact among all the various stakeholders such as the ABC-gate officers, the government, the immigration service, and the research community, respectively. Thus the significance of this thesis are as follows:

1. To give researchers insight into existing algorithms for face morphing attack detection.
2. This study would act as reference material for other researchers who want to conduct further research into MAD problems.
3. This research will aid in minimising the use of fake documents by criminals as forms of identification.
4. This study will aid security officers in catching criminals using morphed e-passport at the ABC gates.

5. Contributes to Face attack analysis by developing a practical MAD technique that can detect morphed face images in the presence of post-processed image sources.

1.6 Organization of the Thesis

This thesis entails of five chapters ranging from Chapter one to Chapter five. The overview of the research is outlined in the first chapter. It consists of the problem statement, aim and objectives, limitations of the study, the study's scope, and study significance. A review of the previous related research works is presented in chapter two. The research methodology is presented in chapter three. This includes the technique of data collection, image analysis, feature processing, and classification. Chapter four presents the details of the actual experimentation conducted and the results obtained compared to existing methods. Conclusions were drawn in chapter five, as well as suggestions for future research.

CHAPTER TWO

2.0 LITERATURE REVIEW

2.1 Introduction

The previous research on Morphing Attack Detection (MAD) is summarised in this chapter. It's crucial setting the stage for the literature review by first commenting on previous works on the broad topic of face recognition, face morphing, and face morphing attack detection. A summary of the analysis of related works is given at the end of this chapter.

2.2 Face Recognition

Face recognition is among the most widely recognised biometric appearances since it is the most common way for people to identify one another (Damer *et al*., 2018a). This technology's usability and ever-increasing accuracy drive its implementation in a varied range of applications like identity management, border control, surveillance and forensics. However, recently researchers found that FRS generalizability upsurges their vulnerability against invasion, for example, spoofing attacks (Mohammadi *et al*., 2018). A precise attack against FRS centered on morphed face pictures, as provided by Ferrara *et al*. (2014), is an extra attack vector vested by the high generalisation abilities. The morphed face attack is discussed in more detail in section 2.3.

2.3 Face Morphing Attack

For a long time, photograph morphing has been a hot topic in image processing research, with a variety of applications, most notably in the movie industry (Wolberg, 1998). In the picture and feature field, morphing methods can be used to construct artificial biometric models that mimic the biometric details of two or more individuals (Busch *et al*., 2019). The created morphed face image will successfully conform to the probe samples of both participating subjects using current Face Recognition Systems (FRS). All

participating subjects can be accurately checked against a morphed face picture saved as a reference in an FRS server thanks to this forgery.

As a result, morphed face photos are a significant challenge to FRSs because they violate the fundamental principle of biometrics, which is the one-to-one relationship between the sample and the subject. In some countries, the applicant submits an analogue or digital face photo for the e-Passport issuance process.

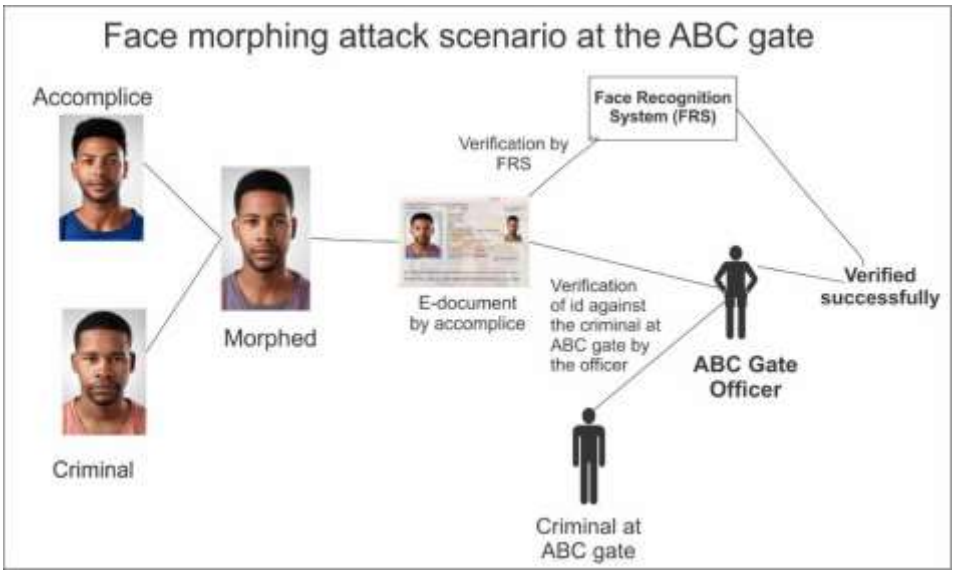

Figure 2. 1 Face Morphing Attack Scenario (Designed by Author)

Figure 2.1 depicts a standard scenario of a face morphing assault. In Figure 2.1, a notorious criminal could morph his face photography with one of his lookalike conspirators. If the partner request for an e-Passport with the morphed face photograph, a new e-Passport with the morphed face photograh will be issued. It's worth noting that morphed face pictures have the potential to fool human examiner (Patel, 2015). The morphed image on the e-Passport could then be used to effectively check both the suspect and his conspirator. As a result of the successful authentication, the perpetrator can now use the e-Passport given to the accomplice to go through the ABC gates (Robertson *et al*., 2018). The risk posed by a face morphing attack is exacerbated because realistic morphed face images can be created by non-professionals using fast face morphing tech that is

either freely accessible, for example, Magic morph, FaceMorpher, WinMorph, and FantaMorph.

2.4 Face Morphing Attack Detection Techniques

Face morphing has been identified as a flaw in Face Recognition System (FRS), and the detection of morphed face images has piqued the attention of academics and industry practitioners who face this problem in their deployed biometric systems (Seibold *et al*., 2018). So many MAD have been proposed in recent years. However, these detection techniques are generally grouped into two key categories (Makrushin & Wolf, 2018). These two classes are the single image-based and differential image-based detection techniques. These broad categories are discussed in subsection 2.4.1 and subsection 2.4.2.

2.4.1 Single Image-Based Detection Techniques

The presence of morph modification on a single image is established in this class, such as the ID photo shown to the officer at registration or the face photo translated from an electronic Machine Readable Travel Document (eMRTD) during gate authentication (Lin *et al*., 2003; Zhou *et al*., 2002). The single given image is processed by the detector and classified as either morph or bona-fide without any reference image (Ramachandra *et al*., 2020). Figure 2.1 presents the single image-based scenario for the face morphing attack. In the single image-based scenario in Figure 2.1, the morphed photo was placed on the e-document, and the face verification system performed attack detection only on the id photo of the presented e-document without matching the id photo with any reference image. The id photo on the e-document was processed by the detector and classified as either morph or bona-fide.

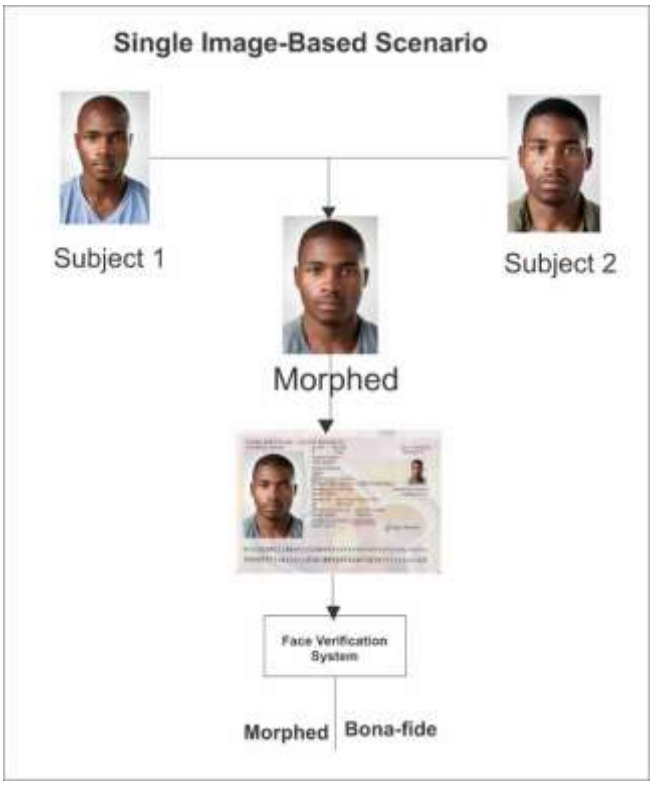

Figure 2. 2 Single Image-based Scenario (Designed by Author)

There are 2 forms of single image-based approaches. These are print-scan attack detection and digital attack detection.

1. **Print-scan Attack Detection:** In this approach, the original images, either morphed or bona-fide, are first printed using a printer and then scanned with a scanner. This method of printing/scanning modifies the image content, eliminating most of the fine details (that is, digital artefacts), which might aid in the easy identification of morphed images (Ferrara *et al*., 2019; Ortega-Delcampo *et al*., 2020; Scherhag *et al*., 2020).
2. **Digital Attack Detection:** Here, the digital copy of the morphed and bona-fide images captured by the camera is being used without undergoing any post-processing like print-scan (Kraetzer *et al*., 2017; Makrushin & Wolf, 2018; Neubert *et al*., 2019; Venkatesh *et al*., 2019a). Digital attack detection is the most frequently used method in the literature.

Several MAD techniques fall under single image-based detection. The majority of previous works on MAD made use of the single image-based detection techniques. The single image-based detection methods are grouped into four (4) broad categories: Texture descriptors, key point descriptors, image degradation descriptors, gradient descriptors and deep features descriptors. These techniques are discussed in-depth in the subsections below.

2.4.1.1 Texture Descriptors

The texture is an essential quality to describe an image. The texture is an attribute utilized to separate images into regions of interest and to categorise those regions. The texture descriptors characterise image textures or areas. The spatial arrangement of colors or intensities in an image or a selected picture region is referred to as texture. Picture morphing alters the textual attributes of morphed pictures, making it a valuable tool for identifying morphed and actual images. The drawbacks of this technique are that it lacks generalization functionality across image resolution and morph data sort, and it performs poorly with post-processed images. Binarized statistical image features and Local Binary Pattern are two common texture-based methods.

a. Local Binary Pattern (LBP)

LBP is a feature descriptor utilised in computer vision classification because of its discriminative capacity and computational straightforwardness (Huang *et al*., 2011). In recent years, the LBP has gained popularity. It is thought to be a reliable texture classification algorithm (Heikkila *et al*., 2009). It works more efficiently when combined with the histogram of oriented gradient descriptor, which rapidly increases the detection performance (Yang & Ai, 2005). LBP is a descriptor that separates an image into pixels. Each pixel in a cell is compared to its neighboring pixel, which is arranged in a clockwise or anticlockwise circular pattern (Nanni *et al*., 2010). The value assigned is 0 if the sum

of the center pixel is higher than the sum of the neighbor pixel; otherwise, 1 is assigned. As a consequence, a binary digit, also known as a binary string, is obtained. The histogram method is then used to generate a collection of pixels that are smaller or larger than the middle. After that, the histogram is normalised (Jeyashree & Deepak, 2018). Texture analysis has made considerable strides thanks to the LBP approach. LBP is a straightforward but powerful texture operator. It has a strong output and is invariant to grey-scale shifts (Song *et al.*, 2013). Assuming a neighbourhood of B sample points on an R radius circle. And a pixel is assigned at (x_p, y_p). LBP can be stated as presented in equation 2.1:

$$\mathrm{LBP}_{B,\mathrm{R}(x_p,y_p)} = \sum_{B=0}^{B-1} \mathrm{C}(i_B - i_P)2^B \quad (2.1)$$

Where i_B and i_p are, independently, gray-level values of the central pixel and P is the surrounding pixels in the circle neighbourhood with R radius, and function c(x) is defined in equation 2.2 as:

$$\mathrm{c(x)} = \begin{cases} 1 & \text{if } x \geq 0 \\ 0 & \text{if } x < 0 \end{cases} \quad (2.2)$$

Spreeuwers *et al*. (2018) performed MAD on single digital images using LBP. The paper aimed at investigating the robustness of MAD methods using cross-database testing. Most reported methods for MAD, according to Spreeuwers *et al*. (2018), are established and validated using a single database of morphed and genuine examples, and frequently high predictive outputs are registered. Using a single image database and morphing software, on the other hand, can lead to a MAD system that only works for this kind of face morphing and not for others.. This work concluded that MAD techniques perform better when used on a homogenous dataset than on cross dataset. One drawback of LBP found by Song *et al*. (2013) is its vulnerability to noise and lighting changes.

b. Binarised statistical image features (BSIF)

It's a feature descriptor generated by binarizing linear filter reactions. The filters are erudite from natural images using independent component analysis, unlike previous binary descriptors (Kannala & Rahtu, 2012). in this technique the code representation of a pixel is called a local representation of the image around the pixel, which signifies a binary code array for an image's pixels. Given an image I_w and a linear filter $F_i$of equal size, the filter response R_i is expressed in equation 2.3.

$$R_i = \sum_{m,n} I_w(m, n)\, F_i(m, n) \tag{2.3}$$

Where *m* and *n* signify the size of the PPI patch and F_i represents the number of linear filters for all $i = \{1, 2, 3, \ldots, n\}$ whose reaction can be computed and binarised to get the binary string in equation 2.4 (Attallah *et al*., 2017).

$$b_i = \begin{cases} 1, & if\ R_i > 0 \\ 0, & Otherwise \end{cases} \tag{2.4}$$

Raghavendra *et al*. (2016) used BSIF to perform MAD. The proposed method used BSIF to obtain a micro-texture variation from a face image, and the classification was done with a linear SVM. The BSIF features of the image are extracted, and the reaction of each pixel to a filter trained on numerical characteristics of natural images is computed in order to represent it as a binary code. With a 1.7% Attack Presentation Classification Error Rate (APCER), the device performed well, demonstrating its usefulness to real life scenarios.The downside of this work is robustness with respect to the dataset used. The dataset was generated using a single morphing tool (GNU Image Manipulation Program), limiting its performance. However, in real-world different morphing tools are used to carry out morphing attack.

2.4.1.2 Key Point Descriptors

These descriptors do not just deal with merely 2D locations on the image but with 3D locations on the image scale space. These locations are the x, y, and scale coordinates.

Key point descriptors are used for MAD, as morphed images are supposed to comprise fewer key point locations described as the maximum and minimal result of Gaussian function difference. Hence the quantity of extracted key points can be used as a valuable feature for MAD. The descriptors in this category include: Speeded Up Robust Features (SURF) and Scale Invariant Feature Transform (SIFT).

a. Scale Invariant Feature Transform (SIFT)

The SIFT descriptor is a feature descriptor used in computer vision to identify and describe local features in images (Lowe, 1999). This descriptor, along with similar image descriptors, is utilized in computer vision for various jobs such as point comparsion between multiple views of a 3-D scene and view-based object recognition. (Scherhag *et al*., 2018c). Since SIFT descriptors are invariant to image domain transformations, scaling and rotations, as well as moderate perspective transformations and illumination variations, they can reliably identify items (Lowe, 1999). In the SIFT algorithm, keypoints are points of interest. At different scales, the image is normalized with Gaussian filters, and the difference between subsequent Gaussian-blurred images is measured. The Difference of Gaussians (DoG) minima/maxima that occur at various scales are then used as keypoints.A DoG image $D(n, m, \mathsf{P})$ is expressed in equation 2.5.

$$D(n, m, \mathsf{P}) = P(m, n, k_i\mathsf{P}) - P(m, n, k_j\mathsf{P}) \tag{2.5}$$

Where $P(m,\ n,\ k\mathsf{P})$ is the convolution of the original image $I(n,\ m)$ with the Gaussian filter $G(m, n, k\mathsf{P})$ at scale $k\mathsf{P}$. The convolution of the original image is shown in equation 2.6.

$$P(n, m, \mathsf{P}) = G(m, n, k_i\mathsf{P}) * I(n, m) \tag{2.6}$$

The DoG image amid scales $k_i\mathsf{P}$ and $k_j\mathsf{P}$ is the dissimilarity of the Gaussian-blurred images at scales $k_i\mathsf{P}$ and $k_j\mathsf{P}$. SIFT Keypoint extractors were used for MAD as morphed

photos are assumed to comprise fewer key locations described as minima and maxima, resulting from the dissimilarity in Gaussians' function.

In Scherhag *et al.* (2018b), different kinds of complimentary feature extraction methods were used to extract features from a single trimmed facial image, including texture extractors (LBP, BSIF), keypoint descriptors (SIFT, SURF), gradient estimation method (HOG), and a deep learning methods. The comparative scores produced by the various extractors were combined using score-level fusion. When compared to using single algorithms, the proposed methodology produced better results..

b. Speeded Up Robust Features (SURF)

SURF is a local feature function identifier and descriptor. some of its applications are: Object detection, labeling, image registration, and 3D reconstruction . (Panchal *et al*., 2013). SURF uses a scale-space description in conjunction with first and second-order differential operators to detect features. To find areas of interest, SURF employs a blob detection technique based on the Hessian matrix. The Hessian matrix's factor is used to quantify local change around a point, and points are selected to maximize this factor (Anjana & Sandhya, 2017; Bay *et al*., 2008). As a feature descriptor, the amount of Haar wavelet responses around the area of focus is used. The integral image can also be used to measure these (Zhu *et al*., 2018). The integral image expressed in equation 2.7.

$$S(x, y) = \sum_{i=0}^{x} \sum_{j=0}^{y} I(i, j) \tag{2.7}$$

The integral image can be used to quickly calculate the quantity of the original image inside a rectangle. This requires assessments at the rectangle's 4 corners. The Hessian matrix $H(p, \sigma)$ at point p and scale σ, given a point $p=(x, y)$ in an image I, is expressed in equation 2.8:

$$H(p, \sigma) = \begin{pmatrix} M_{xx}(p,\sigma) & M_{xy}(p,\sigma) \\ M_{yx}(p,\sigma) & M_{yy}(p,\sigma) \end{pmatrix} \tag{2.8}$$

Where $M_{xx}(p,\ \sigma)$, $M_{xy}(p,\ \sigma)$, $M_{yx}(p,\ \sigma)$ and $M_{yy}(p,\ \sigma)$ are the convolution of the second-order derivative of Gaussian with the image $I(x,\ y)$ at point *p*. For blob-response maps, the box filter of scale 9x9 estimates a Gaussian with a value of σ=1.2 and denotes the lowest point (highest spatial resolution).

2.4.1.3 Image Degradation Descriptors

The feature descriptors in this category take advantage of degradations such as distortion and noise present in images. Image morphing leads to several image degradation due to the morphing process's artefacts, making these degradations important features for MAD. This technique is image compression sensitive and lacks generalization across picture quality and morph data types (digital/print-scan). Photo Response Non-Uniformity (PRNU), Benford characteristics, and Steerable Pyramids are some of the descriptors in this category.

a. Photo Response Non-Uniformity (PRNU)

Sensor Pattern Noise (SPN) is primarily caused by flaws in semiconductor wafer processing and small variations in how individual sensor pixels convert light to an electric signals (Debiasi *et al*., 2018a). Due to the unique characteristics of production flaws and the non-uniformity of photo-electronic transfer, SPN can differentiate imaging sources to the precision of individual devices. The PRNU is the most important component of SPN. The PRNU is a distortion-like pattern that originates from small differences between individual pixels during the photons' digital photosensor transformation into electrons. It's a built-in feature of those sensors, and every image they capture includes this poor signal (Bonettini *et al*., 2018). It's nearly impossible to remove PRNU because of the sensor's physical properties. PRNU is commonly thought of as a feature of a camera's sensor array (Chierchia *et al*., 2011). Fridrich's method can be applied to extract the

PRNU noise residual from a picture. (Fridrich, 2009). For every image *x*, the noise residual R_x is approximated as defined in equation 2.9.

$$R_x = x - D(x) \tag{2. 9}$$

Where D is a denoising operation that removes noise from sensor patterns.

Centered on the PRNU (Photo Response Non-Uniformity) analysis, Scherhag *et al.* (2019a) developed a MAD method. Picture cells were used to analyze the spatial characteristics derived from the PRNU models. At the threshold selection point, the Dresden image database, which was created specifically for PRNU evaluation in image forensics, was used to measure the differences between the attributes of bona-fide and morphed photos. The proposed algorithm was tested on morphed images created using various morphing techniques to reflect a traditional realistic situation, demonstrating its reliability. However, image post-processing procedures such as sharpening, or blurring may have a significant impact on PRNU functionality, reducing the effectiveness of a PRNU-based MAD machine (Debiasi *et al*., 2018a).

A MAD algorithm based on a PRNU analysis was also proposed by Debiasi *et al.* (2018b*)*. It is based on a spectroscopic information of the PRNU's morphing-induced alterations. The wavelet-based denoising filter was used to extract the PRNU for each picture. The frequency distortion reduction (FDR) PRNU amplification is then applied to the extracted PRNU. The Discrete Fourier Transform (DFT) was used to extract the midrange frequencies of the PRNU in each cell as part of the feature extraction process. The magnitude array that results shows the morphing-induced changes in the PRNU signal. A histogram of DFT Amplitudes was determined to reflect the spectrum's magnitude distribution to measure these effects. Since image post-processing activities including sharpening, contrast enhancement, and blurring can have a significant effect on PRNU features, this proposed method investigated the effect of various image post-

processing techniques on detection efficiency. The proposed method was resistant to image scaling and sharpening, with the exception of histogram equalization. To combat the failure to detect morphed images (histogram equalisation), a deeper investigation and improved detection approaches are needed.

b. Benford features

Benford's Law, also well-known as the Law of First Digits, states that the first digits of numbers contained in a sequence of records from a variety of sources do not have a uniform distribution, but rather are organised in such a way that the digit "1" is the most common, followed by "2," "3," and down to "9". It is the likelihood distribution for the first digit's probability in a set of numbers. A random variable satisfies Benford's law if its first digit y occurs with a probability $p(y)$ expressed in equation 2.10.

$$p(y) = \text{nlog}_{10}\left(1 + \frac{1}{\theta + y^{\alpha}}\right), y = 1, 2, 3, \ldots, 9 \quad (2.10)$$

Where θ and α are the parameters specifying the logarithmic curve and n is the e normalisation factor. Ignoring the normalisation factor, the first digits f is computed using equation 2.11.

$$f_i = \left\lfloor \frac{X_i}{10^{\lfloor \log_{10} X_i \rfloor}} \right\rfloor, i = 1, 2, 3, \ldots, K \quad (2.11)$$

Where X_i represent the i-th quantised DCT coefficient and K the amount of DCT coefficients. The Benford features b is expressed in equation 2.12.

$$b_j = \frac{1}{K}\sum_{i=1}^{K} \delta_i, \ \delta_i = \begin{cases} 1 & f_i = j \\ 0 & f_i \neq j \end{cases} \quad (2.12)$$

Benford characteristics can be used in natural data sets for pattern or pattern loss detection (Makrushin *et al*., 2018). The use of Benford's features for pattern detection has led Fu *et al*. (2007) to suggest its use in JPEG format compressed images for tamper detection.

Makrushin *et al.* (2017) used Benford features based on a single image for MAD. In this work, a splicing based approach was used to produce blurred facial images which are visually faultless automatically. A spread of Benford highlights extricated from quantised Discrete Cosine Change (DCT) coefficients of JPEG-compacted transformed pictures were utilised as feature vectors, and the Support Vector Machine (SVM) was applied for grouping. The upside of the suggested system is that it could perform well even on JPEG-compacted transformed pictures. Anyway, the strategy could not distinguish morphed images in the wake of performing print and scan operation on the images. The hypothesis behind applying Benford's characteristics by Makrushin *et al.* (2017) for MAD is that the naturally produced data follow the Benford law, and the altered data infringes the law.

c. Steerable Pyramids

The Steerable Pyramid is concerned with the implementation of linear multi-scale, multi-orientation image decomposition, which is useful for image analysis, object recognition, and machine vision tasks (Simoncelli & Freeman, 1995). The steerable pyramid could be seen as a selective alignment variant of the Laplacian pyramid, during which a steerable filter bank is used at each pyramid level instead of a Gaussian filter. The image goes through the high-pass H_0 and low-pass L_0 filters in a steerable pyramid. The low-pass sub-image is further divided into directed band-pass sub-images utilizing filters $(F_1\ F_2,\ F_3,\ \ldots\ ,\ F_n)$and a lower-pass sub-image using filter L_1 The quantity of bandpass filters is denoted by the letter n. The band-pass constituents are not down-sampled to prevent aliasing in the band-pass section. As a result, in both the horizontal and vertical directions, the lower-pass sub-band is measured by a factor of 2. Incorporating a copy of the shaded portion of the graph at the solid circles spot allows for recursive pyramid construction. This linear decomposition employs a highly restricted series of filters. First,

the filter L_1 should be band-limited, as shown in equation 2.13, to ensure that aliasing terms are eliminated.

$$L_1(\beta) = 0, for\ |\beta| > \pi/2 \tag{2. 13}$$

Consequently, the system's transfer function should also be equal to unity to prevent amplitude distortion. This transfer function is expressed in equation 2.14.

$$|H_0(\beta)|^2 + |L_0(\beta)|^2[|L_0(\beta)|^2 + \sum_{i=1}^{n} |F_i(\beta)|^2] = 1 \tag{2. 14}$$

There is a need for the system to be cascaded recursively; hence another constraint must be verified. This constraint is given in equation 2.15.

$$|L_1(\beta/2)|^2 = |L_1(\beta)|^2[|L_1(\beta)|^2 + \sum_{i=1}^{n} |F_i(\beta)|^2] \tag{2.15}$$

The state of steerability determines the angular restriction on the band-pass filters F_n, which is expressed in equation 2.16:

$$F_n(\beta) = F(\beta)[-jcos(\theta - \theta_n)]^k \tag{2. 16}$$

Where θ, θ_n, and $F(\beta)$ are expressed in equation 2.17, 2.18, and 2.19.

$$\theta = \arg(\beta) \tag{2. 17}$$

$$\theta_n = \frac{n\pi}{k+1} \tag{2. 18}$$

$$F(\beta) = \sqrt{\sum_{i=1}^{N} F_n(\beta)} \tag{2. 19}$$

A steerable pyramid is used for MAD because of its rotational and translational invariance characteristics, which can successfully capture the texture info. This method was used by Ramachandra *et al*. (2020) for MAD. Ramachandra *et al.* (2020) performed MAD by eliminating scale-space highlights with Steerable pyramid, which is a collection of oriented filters created by grouping an elementary function linearly. The Collaborative Representation Classifier (CRC) was used to sort these features. At an APCER of 10%, the suggested methodology produced a Bona-fide Presentation Classification Error (BPCER) of 13.12%. Consequently, even after the print-scan procedure, the proposed

technique was used to perform MAD. Nevertheless, other image post-processing operations such as image blurring, sharpening, and compression were not considered in this paper..

2.4.1.4 Gradient Descriptors

Image gradient is a change of direction in the colour or intensity of the image. These gradient descriptors are used because the morphing process reduces the high frequency of the image and decreases the gradient steepness, enhancing MAD. An example of a descriptor that falls into this category is the Histogram of Gradient (HOG).

a. Histogram of Gradient (HOG)

In image processing, the HOG descriptor is a feature descriptor for object detection and tracking. The method counts the number of times a gradient orientation appears in a given area of an image. This process can be seen in SIFT descriptors, edge orientation histograms, and form contexts. HOG is characterized by its use of alternating local contrast regularization and calculation on a dense grid of equal intervals cells for improved precision (Surasak *et al*., 2018).

HOG features are generated based on the following steps: The picture is first pre - processed and resized. The gradient in the x and y directions is calculated for each pixel in the photo, during which the magnitude and orientation are determined using the formulations in equations 2.20 and 2.21, accordingly.

$$\text{Total Gradient Magnitude} = \sqrt{(G_x)^2 + (G_y)^2} \quad (2.20)$$

Where G_y is the gradient in the y-direction, and G_x is the gradient in the x-direction.

$$\text{Orientation} = tan\ (\theta) = G_y/G_x \quad (2.21)$$

The value of the angle (θ) is presented in equation 2.22

$$\theta = atan\ (G_y/G_x) \quad (2.22)$$

HOG very well adapted for human detection because it is invariant to photometric and geometric transformations (Surasak *et al.*, 2018).

HOG was implemented for MAD by Venkatesh *et al.* (2020). To perform MAD on a single print-scan image, Venkatesh *et al.* (2020) used an aggregate of attributes produced on the scale-space delineation obtained from the color space for the given image. This approach begins by extracting the image's two distinct color spaces. Each of these color images is subjected to a scale-space delineation using the Laplacian transformation with two level fragmentation to capture the high-frequency characteristics. Then an ensemble of features is created using features such as LBP, HOG, and BSIF. The individual morphing scores are obtained using the CRC, and the aggregate of attribute is retrieved individually from each high-frequency frame. Since there are few datasets that describe practical morphing attacks. It was created a new print-scan image dataset of morphed face pictures. Two separate datasets were used in the experiments. For print-scan photos, the proposed technique achieved BPCER = 8.17% at APCER = 5% and BPCER = 5.64% at APCER = 10% on Dataset-1 and BPCER = 6.34% at APCER = 5% and BPCER = 3.77% at APCER = 10% on Dataset-2. However, the technique's generalizability needs further study, including testing on multiple datasets and multiple classifiers.

2.4.1.5 Deep Features Descriptors.

A deep attribute is the coherent layer response within a hierarchical structure to an input that answers relative to the model's final output. Recent research on face recognition has shown that deep features for object recognition and classification have achieved exemplary performance and easy adaptability. These advantages make deep feature descriptors suitable for MAD. Deep feature descriptors suffer from high computational

cost, and training from scratch requires a large database. The convolutional neural network is a popularly used deep feature descriptor for MAD.

a. Convolutional Neural Network (CNN)

The CNN has evolved into a highly effective method of feature extraction and identification in the area of image processing and analysis (Liu *et al*., 2015). CNN is a multi-layer neural net with multiple 2D surfaces in each layer and numerous independent neurons in each plane (Benkaddour & Bounoua, 2017). The architecture of CNN is made up of various kinds of layers, like pooling, fully-connected and convolution layers, and it achieves a kind of regularization (Wandzik *et al*., 2017). Deep architecture is used by CNN to learn complex features and functions that can be used to describe high-level abstractions. Deep architectures are made up of a large number of neurons and multi-level non-linearity calculations. Each level of CNN's architecture signifies attributes at a different abstraction level, which are described as a set of lower-level features (Korshunova *et al*., 2017). The input layer, pooling layers, alternating convolutional layers, and non-linear layers make up the typical CNN structure (Bonettini *et al*., 2018). The feature extraction is handled by the convolutional and pooling layers. fully-connected layers, on the other hand, categories the mined features by the pooling and convolutional layers (Ortega-Delcampo *et al*., 2020).

Raghavendra *et al.* (2017) used a deep neural system as a feasible feature extractor and classifier for MAD. To conduct MAD for print-scan and digital morphed images, the proposed approach used transferrable features obtained from a pre-trained CNN. The feature mining process was carried out using two CNN strategies: VGG19 and AlexNet. The image characteristics were mined separately from the AlexNet and VGG19 models' fully-connected layers. The feature level fusion approach was used to combine these features into a single feature vector. In both cases, the proposed method generated a better

result for digital images with an Equal Error Rate (EER) of 8.22% than print-scan images with an EER of 12.47%. The print-scan post-processing operation, however, was the only one that was considered. Compression, resizing, and sharpening were not taken into account..

Face recognition approaches based on CNN and hand-crafted features are used by Wandzik *et al.* (2018) to solve the problem of MAD. The facial features were mined using four feature extractors. FaceNet, Dlib, and VGG-Face are among these CNN extractors, and the shallow learning approach is based on a High-Dim Local binary pattern. After executing feature extraction using any of the feature extraction process, the extracted features were used to calculate the Euclidean distance for the face verification mission. Using the reference image vectors, the SVM was used to achieve binary classification. The MAD of digital images was only studied in this research, However, the print-scan photos were not considered.

2.4.2. Differential Image-Based Detection Technique

This approach deals with the dissimilarity between a live image (that is, the image obtained at the ABC gate) and the one stored on the electronic record to identify morphed face photographs (Ferrara *et al*., 2019). The basic concept behind this approach is to deduce features from a suspicious morph picture and a live picture taken in a trustworthy environment. To perform MAD, the extracted features are further categorized by calculating the difference between them. Few pieces of literature have explored differential image-based detection approaches. These literature have indicated that introducing a bona-fide reference image permits for a whole new set of technique (Hildebrandt *et al*., 2017). Figure 2.3 presents the differential image-based scenario for the face morphing attack. In differential image-based detection in Figure 2.3, MAD was performed on the morphed image used as an id photo on the e-document by contrasting

the live image (e.g., the image obtained at the gate) with the e-document id photo. The similarity value obtained after determining the detector then classifies the image as either morphed or bona-fide.

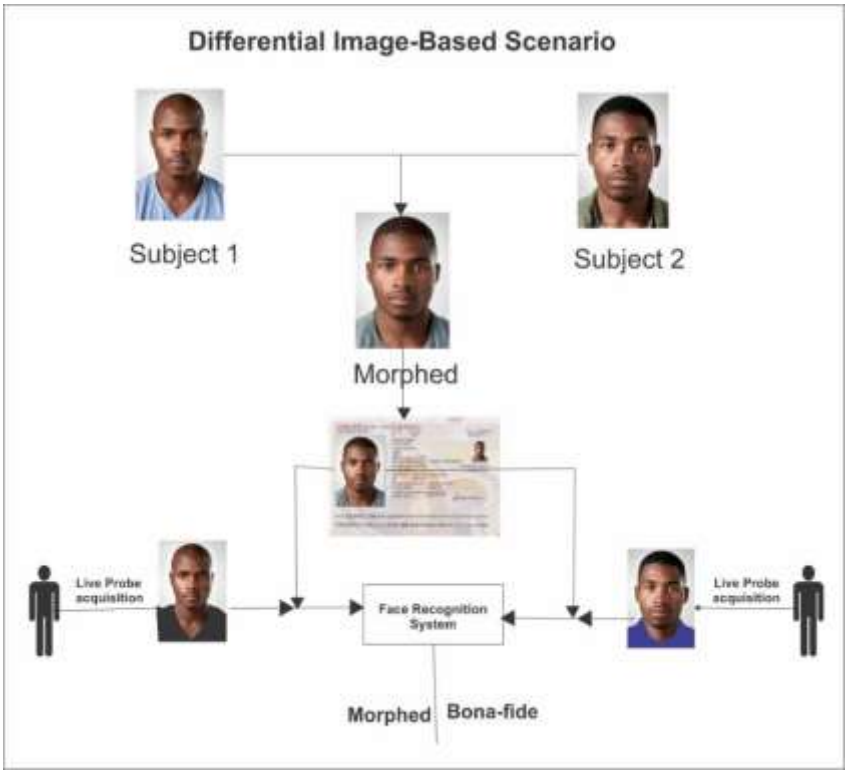

Figure 2. 3 Differential Image-based scenario (Designed by author)

2.4.2.1 Distance-Based Descriptor

The distance-based descriptor is a type of differential-image based detection technique. Distance-based descriptor deals with detecting the landmarks on both the morphed and bona-fide image. The distance of the landmark's relative position between the morphed and bona-fide images is computed, resulting in a feature vector. The calculated distance feature vectors are then used for classification in MAD. The distance-based techniques are used for differential image-based scenarios (Damer *et al*., 2019). This approach deals with the dissimilarity between a live image (that is, the image obtained at the ABC gate) and the one stored on the electronic record for MAD (Ferrara *et al*., 2019).

Scherhag *et al*. (2018a) demonstrated how to use a differential image-based detection method based on comparing the landmarks of a probe (that is, acquired under supervision)

invader picture with the landmarks of the reported picture (that is, the suspected morphed image). The MAD detection was based on the assumption that real-image landmark intra-subject variance is much less than the variance between the morphed photo landmarks and their participating subjects. Two feature extraction techniques were used centered on this premise: distance and angle-based. The next step determines the Euclidean distance between each landmark's relative position in these images (bona-fide image and passport image), producing a feature map of size 2278 known as distance features. The angle-based approach determines the angles of each landmark to a predefined neighbor in order to achieve the most discriminative correlations. The bona-fide photo and the passport image are then compared at the corresponding angles. Return a positive difference between 0^o and 180^o if the angles cross the horizontal line to avoid unrealistically large variations. The 68 variables that make up the resulting function vector are known as angle features. The angles based method produced the best results. However, the classification error rates are not yet small enough for real-world application. Hence in future work, the technique can be combined with a texture-based method to achieve a small classification error rate.

Damer *et al*. (2019) looked at the changing patterns of facial landmarks between reference and probe images to investigate MAD involving a genuine probe image. When comparing the changes caused by normal capture variation to the changes caused by the morphing process, it is presumed that the changes triggered by the morphing mechanism have a discernible pattern. To materialise a result based on this hypothesis, facial keypoints on the reference and probe images were identified, and a landmarks transitions vector to signify their change outlines was calculated.

The Local Binary Pattern Histogram (LBPH) and the transferable CNN were utilized for feature mining. In this work, three detectors were used for landmark mark detection,

namely: an ensemble of regression trees, explicit shape regression and regressing local binary features. The MAD based on landmarks shifts representation based on guided distances was discovered to be superior to the ones discovered by Scherhag *et al*. (2018a) using absolute Euclidean distances. When using total distances, different shift patterns will be linked to the same representation, causing confusion between morphing-induced shifts and naturally occurring shifts caused by capture quality variations. However, further assessments of the impact of perspective distortion applicable in such usage scenarios on landmarks-based attack detection performance are required in this work (Damer *et al*., 2018b). Besides this, innovative morphing attack techniques, such as those centered on generative adversarial networks, that render traditional attack detection approaches vulnerable, have yet to be assessed on this proposed approach (Damer *et al*., 2018a).

A comparative evaluation based on the problem addressed, techniques used, findings, and limitations of related works are presented in Table 2.1.

Table 2. 1 Comparative Evaluation of Related Works

S/N	Author	Detection technique	Approaches Used	Findings	Limitations
1	Venkatesh *et al.* (2019a)	Single image-based	Wavelet Denoising, 3D filtering & Block Matching, Multiresolution Two-sided Filtering. Denoising and Convolutional Neural Networks	A novel MAD approach based on the deep textural characteristics of residual distortion from images was presented. Present a deep MS-CAN for combining four denoising methods and taking into account different noise characteristics.	Focused only on MAD for digital attack without considering the print-scan attack. Image de-morphing was not considered. Extracted only the residual noise without considering texture, keypoint and gradient features.
2	Makrushin *et al*. (2017)	Single image-based	Benford Features	The upside of the suggested system is that it had the option to perform well even on JPEG-compacted transformed pictures	The strategy could not distinguish morphed pictures in the wake of performing print and scan operation on the images.
3	Ramachandra *et al*. (2020)	Single image-based	Steerable pyramid and Collaborative Representation	The majority of the work, particularly with the single image-based methodology, is focused on detecting a digital copy of the morphed face photo. Deep learning techniques based on pre-trained VGG and AlexNet networks were the most explored for MAD.	image post-processing operations such as image compression, sharpening, and blurring were not considered in the proposed algorithm.
4	Scherhag *et al*. (2019a)	Single image-based	PRNU-Based Image Forensics	The algorithm proposed was robust as MAD was performed on morphed images created using various morphing tools representing a typical real-life scenario.	Picture post-processing activities, such as sharpening or blurring, may have a significant impact on PRNU functionality, lowering the effectiveness of a PRNU-based MAD machine.
5	Debiasi *et al*. (2018b)	Single image-based	PRNU-based technique	The proposed method investigated the effects of various image post-processing techniques on detection efficiency, finding that the proposed detector was resistant to image sharpening and scaling.	The system failed for MAD on morphed images processed with histogram equalisation

Table 2.1 Comparative Evaluation of Related Works (Continues)

S/N	Author	Detection technique	Approaches Used	Findings	Limitations
6	Raghavendra *et al*. (2017)	Single image-based	VGG19 and AlexNet	The proposed method accomplish a better result for digital images with an Equal Error Rate (EER) of 8.223% compared to the print-scan pictures with an EER of 12.47%.	The MAD could not attain an outstanding EER for MAD in the print-scan image compared to the digital images.
7	Zhang *et al*. (2018)	Single image-based	Discrete Fourier transformation (DFT) of Sensor Pattern Noise (SPN) and Support Vector Machine	It was identified that the Sensor Pattern Noise (SPN) as features makes a great fit for MAD due to the distinction in the vitality circulation of SPN	Only considered MAD of digital images without consideration of post-processed images
8	Jassim and Asaad (2018)	Single image-based	Topology Data Analysis (TDA) Collaborative representation classifier	The Topology properties of constructed shapes from a given Photo ID faces provided good features for MAD.	The system performed poorly on print and scan images
9	Ferrara *et al.* (2019)	Single image-based	Deep Neural Networks (AlexNet and VGG)	Provided solution to deal with cross-database testing and printed-scanned images. In the presence of Print-scan photographs, it was found that more advanced and face-specific filters were required to identify the fine details artefacts that survived the print-scan process.	MAD in the Print-scan images was not as high as the digital images. Only print-scan was considered as a post-processing operation
10	Singh *et al*. (2019)	Single image-based	CNN (pre-trained AlexNet)	A new database of morphed images and trusted live capture probe images captured in a realistic border crossing scenario using ABC gates is presented. Proposed a new method for detecting morphing attacks that uses a combination of scores from a quantized normal-map phase and dispersed reconstructed image features to exploit the intrinsic border crossing situation.	This paper's impediment is that the proposed algorithm did not consider picture post-processing tasks, such as the print-scan operation, image compression, sharpening, and blurring.

Table 2.1 Comparative Evaluation of Related Works (Continues)

S/N	Author	Detection technique	Approaches Used	Findings	Limitations
11	Wandzik *et al*. (2018)	Single image-based	faceNet, Dlib, VGG-Face, High- Dim Local binary pattern, and SVM	Instead of adding new components, the proposed approach makes use of an established feature extraction pipeline for face recognition systems. It doesn't need any fine-tuning or changes to the current recognition scheme, and it can be trained with a small dataset.	This study only looked at the MAD of digital images, not the print-scanned images that are used for authentication in some nations.
12	Scherhag *et al.*(2018b)	Single image-based	LBF, BSIF, SIFT, HOG and CNN	MAD output can be significantly improved using a multi-algorithm score-level combination that maximizes the discriminative power of processed data.	Used a single tool for morph, limiting the diversification of the dataset and reducing the proposed algorithm robustness.
13	Scherhag, *et al.* (2018a)	Differential image-based	Distance-based (Euclidean) and Angle- based	Demonstrates the use of a differential image-based detection technique based on variation between the landmarks of a probe bona-fide image of the intruder and the landmarks of the registered image.	The classification error rates are not yet small enough for real-world application. Hence in future work, the technique can be combined with a texture-based method to achieve a small classification error rate.
14	Venkatesh *et al.* (2020)	Single image-based	LBP, HOG and BSIF	Given the limited availability of datasets representing realistic morphing attacks. A new print-scan image dataset of morphed face images was generated.	The generalizability of the technique needs further investigation with an evaluation of multiple datasets and multiple classifiers.
15	Damer *et al.* (2019)	Differentia l image-based	LBPH and transferable CNN	MAD using landmark shifts representation based on directed distances outscored MAD using absolute Euclidean distances This is due to the fact that by using absolute distances, various shift patterns are translated to the same representation, causing uncertainty between morphing-induced shifts and naturally occurring shifts caused by capture quality variations.	However, more research is needed on the impact of perspective distortion, which is relevant in such use situation, on the performance of landmarks-based attack detection in this work.

16	Raghavendra *et al.* (2016)	Single image-based	BSIF	The system attained a good performance with APCER of 1.73% that shows its applicability to a real-world scenario.	The downside of this work is robustness with respect to the dataset used. The dataset was generated using a single morphing tool (GNU Image Manipulation Program), limiting its performance.

2.5 Summary of Related Works

In this chapter, face recognition and morphing were discussed. The strength and weaknesses of the methods used in previous related works for MAD were identified. This review's findings reveal a lack of significant extant literature on the specifics of the investigation topic (Post-process image sharpening) for this research. When considered together, it is clear that previous studies on MAD are not robust in dealing with post-processed image sources.

CHAPTER THREE

3.0 METHODOLOGY

3.1 Introduction

The techniques used to conduct this research are described in this chapter. It provides information on the generation of the dataset used. The research process that was chosen for this study is presented. A comprehensive discussion of the data collection and generation, image post-processing and pre-processing, feature extraction, dimensionality reduction, feature fusion and data classification are presented. Lastly, the evaluation metrics used to validate the proposed system are also discussed.

In this thesis MATLAB environment was used as the implementation and evaluation environment. The proposed solution is illustrated in Figure 3.1, and this solution is discussed in detail in this chapter.

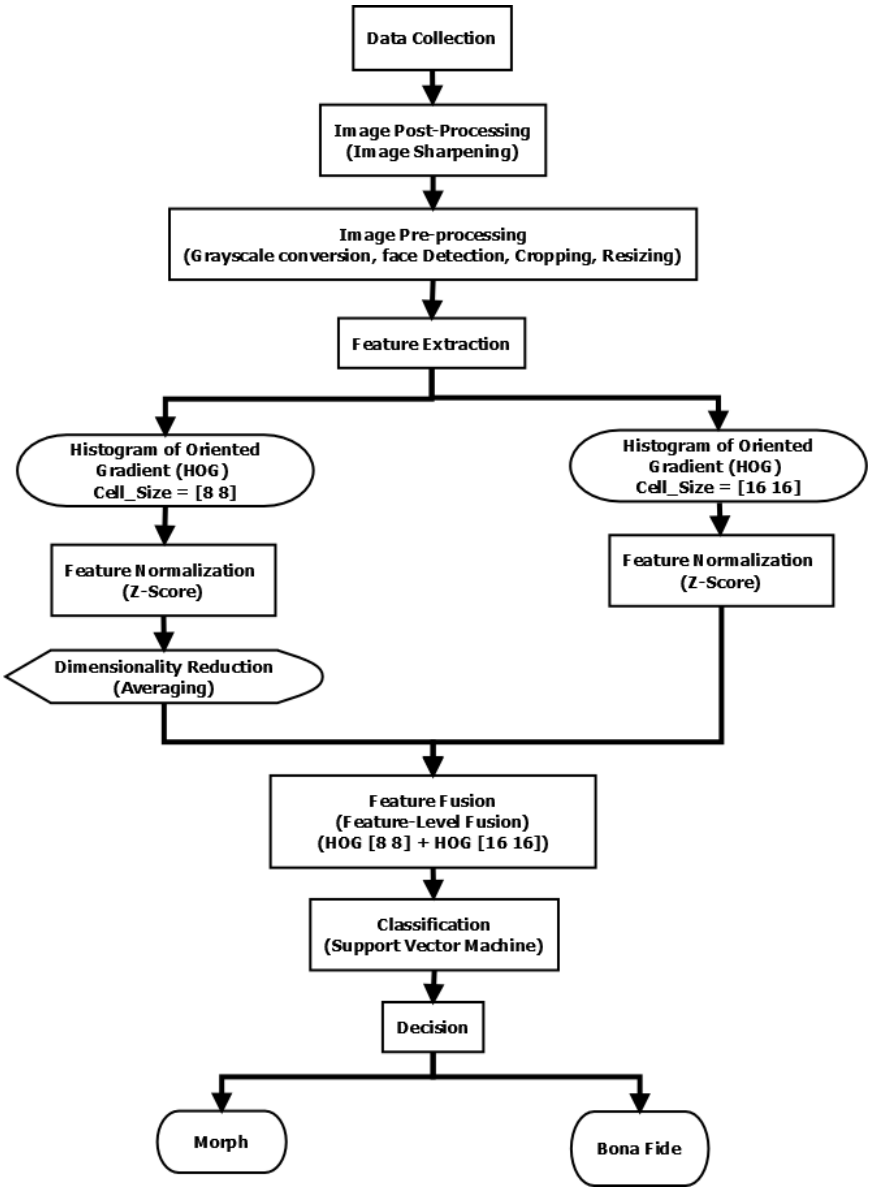

Figure 3. 1 Proposed Technique

3.2 Data Collection

In this research, an unique morphed face database of 200 morphed photos and 150 bona-fide photos was created utilizing various facial photos from 100 subjects, totaling 350 images. Male, female, white and dark skin individuals were included in the face pictures to help diversify the database. The images for the subjects came from a variety of online sources, including the Yale Face Database (“Yale Face Database,” 2020) and the 123RF photo website (123RF, 2020).

The morphed face images were created with the help of two morphing tools:

1. **Magic morph software:** This is a free Windows-based program that acts as a useful image and graphics utility for users. It is high-speed morphing and warping program. Magic Morph allows users to animate their still images into SWF, GIF, or AVI files with morphing effects. It is easy and straightforward to use. Quick and multithread pyramid methods, expert-quality warping and morphing techniques, and real-time visualization functions are all included in the app. TIFF, BMP, JPEG, J2K, PNG, ICO, GIF, TGA, WBMP, PCX, WMF, and JBG are among the file formats supported by this method. Its compatible output files, on the other hand, are AVI, GIF and SWF Movie, JPEG and BMP Sequence. Figure 3.2 shows the interface of Magic Morph software after loading the subject images.

Figure 3. 2 Magic Morph Interface after loading subject images

2. **FantaMorph software:** This is a transforming app that can be used to create photo transformations and modern transform activity effects. It assists users in locating facial features such as the eye, nose, and mouth, and then combines these features from different real-life faces to produce a virtual face. FantaMorph is available in three editions: Standard, Professional, and Deluxe, and supports both Windows and Mac operating systems. Figure 3.3 shows the FantaMorph tool

interface after loading subject 1 and subject 2 images shown in the up row. While in the down row is the morphed face image before manual adjustment and merging to remove the artefacts.

Figure 3. 3 FantaMorph tool after load subject 1 and subject 2 images

In Figure 3.4, the two images on the upper row show manual points (green) on subject images used for blending the two subject images. And the single image in the lower row shows the blended image.

Figure 3. 4 FantaMorph interface after performing manual merging and blending of subject images

Figure 3.5 is a morphed image without the manual merging of points for proper blending to cloak artefacts. Plate I is the same morphed image in Plate II after manual blending has been performed on the image.

Plate I Morph image before manual blending

Plate II Morph image after manual blending

To cover the altered antique, the face pictures were manually balanced and combined. The morphing program produces a series of picture outlines that demonstrate how one subject changes into another. During the transforming process, the last transformed image is manually selected based on its resemblance to the faces of the contributing subjects. As a result, the produced transforms are of high quality and have few if any discernible artefacts.

Plate III Subject 1(123RF, 2020)

Plate IV Subject 2 (123RF, 2020)

Plate V Morphed

Plate VI Sharpened image

Plate III shows an image of subject 1: which is the image of one of the individuals making up the morphed image; Plate IV shows a picture of subject 2: which is the image of the second individual making up the morphed image; Plate V is the morphed image: this is the combined image of subject 1 and 2 using a morphing tool; Plate VI is sharpened morph image: this is the morphed image in Plate V after carrying out post-processing task on the image.

3.3 Post-processing (Image Sharpening)

Before being loaded into an e-visa, the photographs used in identification documents would pass through various scanning operations. After being post-processed, a morphed image loses a lot of its artefacts, making MAD of such photographs difficult. Two common image post-processing techniques are image sharpening and compression. Image sharpening is a typical image post-processing procedure since human vision is highly sensitive to edges and subtleties in a picture. Since pictures are often made up of high-frequency sections, the graphic quality would suffer if the high frequencies are distorted. When the high-frequency fragments of a picture are enhanced, the visual picture

quality increases. Sharpening morphed images can also highlight edges and adjust background intricacies, as well as change the morph highlights, making the image difficult to detect. One of the challenges in MAD, according to Scherhag *et al*. (2019b), is image sharpening. As a result, picture sharpening was applied to the morphed photos in order to improve their identification and evoke the proposed MAD method's efficacy even after conducting post-processing operations for image enhancement. A sharpened morph image is shown in Figure 3.10.

3.4 Face pre-processing

In the face pre-processing stage, four operations were carried out. These operations include Facial landmark detection, cropping, image resizing and Gray-scale conversation. Each of these processes is discussed in details in the subsections below.

3.4.1 Facial Landmark Detection

Facial landmarks were detected during the pre-processing step. The problem of detecting facial landmarks is a branch of the shape prediction problem. A shape predictor uses an input image to try to locate key points of interest. Facial landmarks, like the eyes, nose, mouth, jawline, and brows are used to confine and denote visible areas of interest (Seibold *et al*., 2017). The following are the two (2) measures involved in identifying facial landmarks:

- Step 1: Determine the location of the object of interest (face).
- Step 2: Identify the main facial features on the face region of interest.

The Viola-Jones technique was used to discover face features in this study. The Viola-Jones method was chosen due to its high discovery rate and low false-positive rate, as well as its limited use for face detection. The Haar-basis filters, which are a scalar object among the photo and some Haar-like designs, are used in the Viola-Jones computation. (Wang, 2014).

The Viola-Jones face detection algorithm is divided into four phases: Haar feature selection, integral image selection, Adaboost training, and cascading classifier (Viola & Jones, 2001). The input image is first converted into an integral image by the Viola-Jones face detection process. The integral image is a method for generating the number of pixel distributions in a rectangle in a photograph in an operational manner.

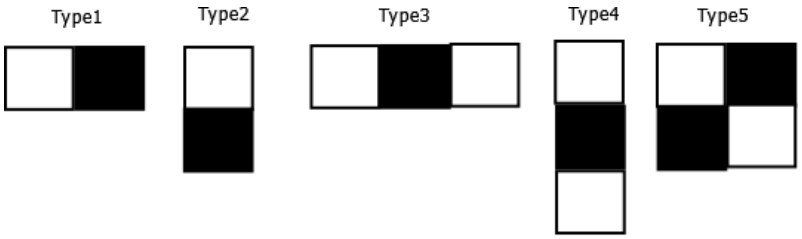

Figure 3. 5 Haar features (Viola & Jones, 2001)

Figure 3.5 depicts the various types of characteristics. The Haar features in Figure 3.5 have different height and width. Figure 3.5 shows how the image is depicted using either black and white pixels. By deducting the sum of the white rectangles from the sum of the black rectangles, each function yields a single value. If the calculated value is higher in that area, it denotes a facial feature such as the eyes, nose, jawline or mouth (Jensen, 2008). AdaBoost is an enhancing algorithm for machine learning that can build a strong classifier from a weighted mixture of weak classifiers (A weak classifier correctly categorizes just somewhat more than half of the instances). By identifying the important and insignificant features, Ada boost reduces the number of redundant features. Following that, the Ada boost assigns weight to all of them after distinguishing the essential and unimportant features. As a result, of linear clustering of weak classifiers, a robust classifier is created. Any feature is regarded as a possible weak classifier. Equation 3.1 describes a weak classifier statistically.

$$h(y, f, s, \emptyset) = \begin{cases} 1 & if\ sf(y) > s\emptyset \\ 0 & otherwise \end{cases} \quad (3.1)$$

Where y is a 24-by-24-pixel sub-window, f is the implemented feature, s is the polarity, and $\emptyset$ is the threshold for classifying y as positive (a face) or negative (a non-face)

(Deshpande & Ravishankar, 2017). A total of nearly 2500 features are being estimated. Cascading is thus used to decrease the number of computations needed. A strong classifier is present at each stage of the cascaded classifier. Each stage's goal is to decide if a particular sub-window is certainly not a face or may be a face. A sub-window is automatically discarded when it is labeled as a non-face by a given point. On the other side, a may be face sub-window is progressed to the next stage of the cascade. As a consequence, the more phases a sub-window passes through, the more likely it is to include a face. Figure 3.6 illustrates the principle with three steps.

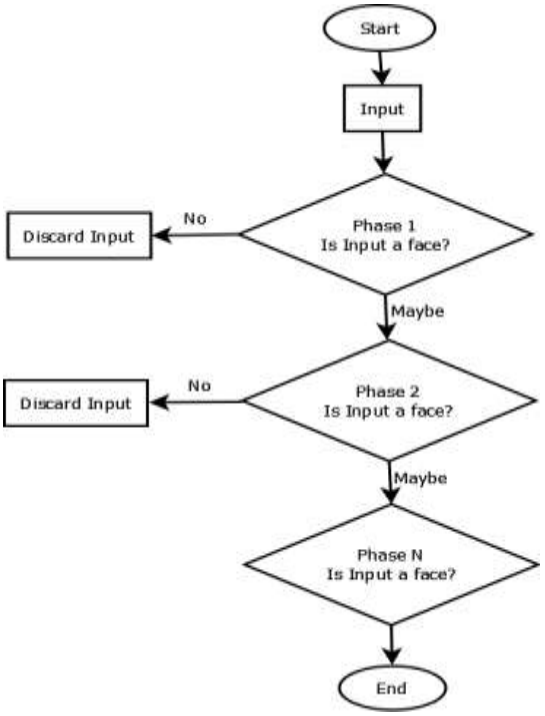

Figure 3. 6 The Cascaded Classifier (Deshpande & Ravishankar, 2017)

To decrease the false positive rate in a single stage classifier, one must usually consider false negatives. False positives aren't regarded a concern in the early stages of the staggered classifier, but they must be addressed later on. As a result, Viola-Jones recommends taking a high number of false positives into account at first. As a consequence, the number of false negatives for the final phased classifier is predicted to be very low. The cascading classifier is also known as a perceptual cascade by Viola-Jones. This name refers to the fact that more emphasis (computing power) is placed on

areas of the image that are assumed to contain faces. Plate VII shows a face image with the detected facial features after performing face detection using voila jones algorithm.

Plate VII Detected facial features using Voila Jones

3.4.2 Image Cropping

Cropping is the removal of a photographic image from unnecessary external areas. The method usually entails removing any of the image's peripheral areas in order to remove extra garbage, improve framing, change the aspect ratio, or highlight or isolate the subject matter from its context.

The face images were cropped to magnify the primary subject (face) and further reduce the angle of view to a scale of 130 by 130 pixels founded on the identified landmarks to guarantee that the MAD procedure is only utilized on the facial area after the facial landmarks were identified using the Voila Jones algorithm.

Plate VIII Input face Image (123RF, 2020)

Plate IX Face Image after Performing cropping operation

Plate VIII shows the original input face image before performing the image pre-processing operation. Plate IX illustrate the face image in Plate VIII after performing the cropping operation on the detected face region.

3.4.3 Grey-Scale Conversion

A grey-scale image in digital image processing is one in which a single sample representing only a quantity of light is the value of each pixel; that is, it holds only intensity values. The pictures in grey-scale, a kind of grey monochrome, are made entirely of shades of grey. At the lowest intensity, the contrast varies from black to white at the highest (Saravanan, 2010).

The grey-scale conversion process removes all color information, leaving only the luminance of each pixel. Each pixel has three different luminance values because digital photography uses a combination of red, green, and blue (RGB) colours. These 3 values must also be combined into a single value when extracting colour from an image (Kumar & Verma, 2010).

In this phase, the cropped RGB or coloured face images were converted to a grey-scale image to prepare the images for feature extraction.

Plate X Cropped Morphed Image

Plate XI Cropped Bona-fide Image

Plate X shows a cropped morphed image: that is, a cropped morphed image based on the discovered facial landmarks. Plate XI shows a cropped bona-fide image: that is, a cropped bona-fide image based on the identified facial landmarks.

3.4.4 Image Resizing

The graphic primitives constituting a vector graphic image can be sized using geometric transformations without losing image quality when resizing it. Image resizing can be interpreted as image reconstruction (Dong *et al*., 2012; Malini & Patil, 2018). The image

size can be changed in several ways, but the Nearest- neighbour interpolation (NNI) algorithm was adopted in this work. NNI is a straightforward approach for interpolating multivariate data in one or more dimensions. The nearest neighbour method assigns the value of the nearest point without taking into account the values of neighboring points, resulting in a piecewise constant interpolate (Olivier & Hanqiang, 2012). The NNI algorithm is one of the more straightforward ways of increasing image size. This deals with exchanging every pixel in the output with the nearest pixel; for up-scaling, this ensures there will be several pixels of the same color. Pixel art may benefit from this because sharp details can be preserved. (Parsania & Virparia, 2016).

In this step, the cropped images were all resized to the same scale to enable extraction of the same number of feature vectors.

3.5 Feature Extraction

Feature extraction is a technique for reducing dimensionality. This method divides and reduces an initial set of raw data into more manageable classes. This action simplifies image analysis. A common and significant feature of images is their large number of variables. A huge proportion of computational power is required to handle these variables. As a result, feature extraction helps in the retrieval of the best feature from large amounts of data by selecting and integrating variables into features, thus reducing the dimensionality of data (Choras, 2007). These features are simple to use while still accurately and uniquely describing the data collection. The reduction of data makes it easier for the algorithm to construct the model with little effort and speeds up the learning and generalization steps in the machine learning process (Kumar & Bhatia, 2014).

The Histogram of Oriented Gradient (HOG) function descriptor was used to extract the desired features from both the morphed and genuine photos.

3.5.1 Histogram of Oriented Gradient (HOG)

The HOG is a feature descriptor for object recognition in image processing. The technique counts the number of times a gradient orientation occurs in a specific area of an image. This method is demonstrated by scale-invariant aspect transform descriptors, edge orientation histograms, and shape contexts. It stands out because it is built on a condensed array of evenly spaced cells and uses overlap contrast enhancement for improved accuracy (Suard *et al*., 2006).

The following is how the HOG features are made: The variance in the x and y directions for each pixel in the picture is calculated after preprocessing and resizing the image, and the orientation and magnitude are computed using the formulas in equations 3.2 and 3.3, accordingly.

$$\text{Total Gradient Magnitude} = \sqrt{(G_x)^2 + (G_y)^2} \tag{3.2}$$

Where G_y denotes the y-direction gradient and G_x denotes the x-direction gradient.

$$\text{Orientation} = tan\ (\theta) = G_y/G_x \tag{3.3}$$

The value of the angle (θ) is presented in equation 3.4

$$\theta = atan\ (G_y/G_x) \tag{3.4}$$

HOG is unaffected by photometric and geometric transformations, making it ideal for object recognition (Dalal & Triggs, 2005). The HOG gradient descriptor was used in this study because the image morphing process reduces the changes in the high frequency of the image and decreases the morphed images' gradient steepness, enhancing MAD.

HOG works by dividing the image window into tiny spatial regions called "cells." Over the cell's pixels, each cell accrues a local 1-D histogram of descent directions. Based on the cell size, two types of HOG features were extracted in this study. The HOG cell size used were 8x8 pixels and 16x16 pixels.

There are no optimal values or scale in HOG feature description to extract the best feature for classification. For example, cell size 8 x 8 is HOG with fine cells. But perhaps it is not the best scale (because the cells are too small and noise might just be observed) (On the other hand, too large cells, like cell size 16 x 16, maybe too large, and there will have uniform histograms everywhere). The best way to obtain the best features is by extracting HOG at various scales and combining them. Hence the 8 x 8 pixels cell size was used to capture small-scale spatial information from the images, while 16 x 16 pixels cell size was used to capture large-scale spatial details from the pictures.

The HOG with 16 x 16 pixels cell sizes consists of 648 feature vectors. The HOG with 8 x 8 pixels cell sizes consists of 4320 feature vectors.

3.6 Feature Normalization

Normalization is the process of converting values calculated on various scales to a nominally uniform scale, which is often done before averaging. The method of feature normalization is used to normalize the range of independent variables or data attributes. The purpose of normalization is to convert attributes to be on a comparable scale. This increases the reliability of the models' performance and training (Kumar *et al*., 2015).

Distance algorithms like KNN, SVM, and K-means are mainly affected by the selection of features. This is because they compare data points by measuring the distance between them (İLeri *et al*., 2018). Therefore, the data was scaled before employing SVM so that all the features contribute equally to the result.

The extracted features were normalized to ensure that the HOG(8x8) and (16x16) feature vectors were on the same scale and contributed equally to the classification result. The Z-Score normalization technique was used to normalize the extracted features.

3.6.1 Z-Score

A prevalent technique to normalize features to zero mean and unit variance is the Z-score normalization technique (Shalabi *et al*., 2006). The Z-Score is an arithmetical metric for comparing a score to the mean of a group of scores (Kolbaşi & Ünsal, 2015). Z-Score is calculated based on the formula in Equation 3.5.

$$Z_{score}(i) = \frac{x_i - \mu}{s} \tag{3.5}$$

Where s= standard deviation, μ = distribution mean, and x_i = each object in the distribution. Equation 3.6 provides the formula for calculating the standard deviation:

$$s = \sqrt{\frac{1}{n-1}\sum_{i=1}^{n}(x_i - \mu)^2} \tag{3.6}$$

3.7 Averaging Dimensionality Reduction and Feature Fusion

Dimensionality reduction is the transition of data from a high-dimensional structure to a low-dimensional structure in such a way that the low-dimensional model retains some significant features of the data sources, preferably close to its fundamental dimension (Sembiring *et al*., 2011; W. Yang *et al*., 2012).

3.7.1 Averaging Dimensionality Reduction

In this study, dimensionality reduction was performed as an intermediate step to facilitate the feature fusion process. Feature Fusion is a technique for combining similar data extracted from a collection of training and testing images without losing any detail (Gawande *et al*., 2013; Sudha & Ramakrishna, 2017).

Dimensionality reduction was performed only on HOG 8 x 8 pixels cell size. The HOG 8 x 8 pixels cell size consisting of 4320 features was reduced to consist of 648 features. Dimensionality was performed using averaging. Averaging was used to ensure that every initial HOG 8 x8 features contributed to the new reduced features. The averaging dimensionality reduction was performed on HOG 8 x 8 features because summation

feature-level technique can only be applied to different features of the same dimension. Hence, the dimensionality of the HOG 8 x 8 features must be equal to the HOG 16 x 16 features' dimensionality.

To average the HOG 8 x 8 features, the features were divided by the number of HOG 16 x 16 features. The result of this division was used to group the features for averaging. For example the 4320 (number of HOG (8 x 8) features) was divided by 648 (number of GLCM features) which results to approximately 7. This means that the first seven (7) features will be averaged first, followed by the next 7 features. Averaging of each 7 feature continues till the 4320th feature. The algorithm for dimensionality reduction and feature-level fusion technique is presented in algorithm 3.1.

Algorithm 3.1 Averaging Dimensionality Reduction And Feature Fusion

Inputs:

$H_8[] = \{X_1, X_2, X_3, \ldots, X_n\}$ *//HOG (8 x 8 cell size) feature vectors*

$H_{16}[] = \{Y_1, Y_2, Y_3, \ldots, Y_n\}$ *//HOG (16 x 16 cell size) feature vectors*

Output:

F[] *//Fused feature of $H_8[]$ and $H_{16}[]$*

1: get number of rows for $H_8[]$,*n_rows*

2: get number of columns for $H_8[]$, C_1

3: get number of columns for $H_{16}[]$, C_2

4: $M_1 = \text{floor}(C_2/C_1)$ *// get floor value for C_2 divided by C_1*

5: $N_1 = C_2 - (M_1 * C_1) + M_1$ *//to get first set of columns to average*

6: ***for*** *i = 1 to n_rows //Looping through rows*

7: $Q_1 = \text{mean}(H_8(1 \text{ to } N_1))$ *// to average the selected first set of columns for $H_8[]$ features*

8: ***for*** *$t = N_1 + 1$ to C_2 //Loop through the group columns and /increment by M_1*

9: $Q_1 = \text{Concatenate}(Q_1, \text{mean}(H_8(t \text{ to } t + M_1 - 1))$ *//merge the average of the first, second, third, fourth, …C_1 selected set of columns for H[] features*

10*:* ***end***

11: ***end***

12: $\sum H_{16}[] \, Q_1$ *//average Feature fusion for $H_{16}[]$ and reduced dimension $H_8[]$*

13: *F[] = Concatenate ($H_{16}[], Q_1$)*

14*:* *return F[]*

The reduced 8 x 8 cell HOG features was fused with HOG 16 x 16 features to produce a 648 features. Given HOG (8 x 8 cell) and HOG (16 x 16 cell) features as $H_8 = \{X_1, X_2, X_3, \ldots, X_n\}$ and $H_{16} = \{Y_1, Y_2, Y_3, \ldots, Y_n\}$ respectively. H_8 feature dimension were reduced to H_{16} dimension using the formula in equation 3.7 and equation 3.8.

$$Q_1 = \text{mean}\ (H_8\ (1 \text{ to } N_1) \tag{3.7}$$

$$Q_1 = \text{Concatenate}\ (Q_1, \text{mean}\ (H_8\ (t \text{ to } t + M_1 - 1)) \tag{3.8}$$

Q1 is the reduced H_8 dataset and the average of the first set of selected columns, t is the second set of selected columns, and n is the last column of the original H_8 dataset.

3.7.2 Feature Fusion

Feature Fusion is a technique for combining similar data extracted from a collection of training and testing images without losing any detail (Gawande *et al*., 2013; Sudha & Ramakrishna, 2017). Summation feature-level technique was used for fusion. The summation feature-level technique is expressed in equation 3.9 and 3.10. The summation feature-level fusion formula to fuse H_8 and H_{16} is presented in equation 3.9.

$$\sum H_{16}\ Q_1 \tag{3.9}$$

The fused H_8 and H_{16} were then concatenated to produce the final feature vectors using the formula in equation 3.10.

$$F = \text{Concatenate}\ (H_{16}, Q_1) \tag{3.10}$$

The new set of concatenated feature vectors (648 features) generated using the summation feature level fusion technique were used to train the SVM classifier.

The main advantage of feature-level fusion is that it detects correlated feature values produced by different feature extraction methods, resulting in a compact collection of salient features that can boost detection accuracy (Bhardwaj, 2014).

3.8 Image Classification

Classification is the process of deciding which of a set of categories a new observation belongs to based on a training set of data that includes observations with existing classification membership (Azhar & Thomas, 2019). To put it another way, image classification is the method of categorizing and marking groups of pixels or vectors within an image according to a set of laws. One or more spectral or textural characteristics may be used to create the categorization rule (Shinozuka & Mansouri, 2009). An excellent illustration of supervised learning is classification (that is, learning in which a set of accurately categorized observations are used as a training set) (Mills, 2011; Kalapatapu *et al.*, 2016). A classifier is a system that implements classification, particularly in a concrete implementation.

In this work the SVM classifier was utilized to categorize the face images into morph or bona-fide images.

3.8.1 Support Vector Machine (SVM)

SVM is a supervised learning framework with related learning algorithms for regression and classification analysis (Meyer *et al*., 2003). The SVM technique seeks to locate a hyper-plane in a D-dimensional domain (where D denotes the number of features) that distinguishes between data sets (Chih-Wei & Chih-Jen, 2002). Hyperplanes are decision lines that aid in data classification. Different groups can be assigned to data points on either side of the plane. The hyperplane's dimension is also determined by the number of functions. The hyperplane is just a line if there are only two input features. When the number of input features exceeds three, the hyperplane becomes a two-dimensional plane. SVM has a number of advantages, one of which is its adaptability (that is various Kernel functions can be defined for the decision function) (Crammer & Singer, 2001). In the input space, the decision function of a binary SVM is represented in equation 3.11:

$$\gamma = h(x) = sign\left(\sum_{j=1}^{n} u_j y_j K(x, x_j) + v\right) \quad (3.11)$$

where *x* is the feature vector to be classified, *j* is the training instance index, n is the number of training examples, and y_j is the training example label (1/ –1). u_j and v are fitted to the data to optimize the margin, and j, K(,) is the kernel function. Training vectors are training vectors for which $u_j \neq 0$ is zero (Sopharak *et al*., 2010). This study makes use of SVM for binary classification as SVM are primarily designed for 2-class classification problems (either morphed or bona-fide). SVM considers two approaches which are case when data are linearly separable and case when the data are non-linearly separable.

3.9 Performance Metrics

The following evaluation metrics were used to approximate the efficiency of the proposed technique.

1. **FAR (False Acceptance Rate)**: This is the same as the APCER. It is defined as a percentage of morphing attack that is classified as bona-fide images (Ramachandra *et al*., 2020). Equation 3.12 contains the formula for FAR.

$$\text{FAR} = \text{FP}/(\text{TP} + \text{FP}) \quad (3.12)$$

2. **FRR (False Rejection Rate):** This is the same as the BPCER. The FRR is defined as the proportion of bona-fide presentations incorrectly classified as presentation attacks in a given situation, or the proportion of bona-fide images incorrectly classified as morphing attacks (Wandzik *et al*., 2018). In equation 3.13, the FRR formula is given:

$$\text{FRR} = \text{FN}/(\text{TP} + \text{FN}) \quad (3.13)$$

3. **ACC (Accuracy):** This is a metric for assessing classification models' reliability. Accuracy can be clearly defined as the percentage of correct classifications for an independent test set (Ferrara *et al*., 2016). In equation 3.14, the formula is given:

$$\mathrm{ACC} = \frac{\mathrm{TP} + \mathrm{TN}}{\mathrm{TP} + \mathrm{TN} + \mathrm{FP} + \mathrm{FN}} \tag{3.14}$$

4. **Detection Error Tradeoff (DET) Curve:** This is a graphical representation of error rates for binary classification systems that plots the false rejection rate versus the false acceptance rate.

Where FN = False Negative, FP = False Positive, TP = True Positive and TN = True Negative.

3.10 Implementation Tool (MATLAB)

The MATLAB environment was used to carry out image post-processing, image preprocessing, feature extraction, dimensonality reduction, feature fusion, classification and evaluation. MATLAB stands for Matrix Laboratory, and all of the infrastructure of MATLAB is matrix-based. In terms of engineering, computations, simulation, image analysis, and other tasks, MATLAB is one of the most extensively used engineering tool. This software is utilized for academic purposes, particularly scientific research, due to its ease of use in comparison to other classic languages such as FORTRAN, C, and C++. The MATLAB environment is not a standalone executable, but rather a pre-packaged software package that includes a set of tools and capabilities for data analysis and visualization. The MATLAB version used in this thesis is R2018a.

CHAPTER FOUR

4.0 RESULTS AND DISCUSSION

4.1 Introduction

The results of using the proposed technique and several other techniques on both post-processed morphed and bona-fide images as well as non-post-processed morphed and bona-fide images are presented in this chapter. After each presented result, a detailed explanation or discussion of each obtained result is given below the chart or table depicting the result.

4.2 Results and Discussion

In this research the face image dataset was divided into two for training and testing. 80% of the dataset was used for training while the remaining 20% datasets were used to test the model.

In this research experiments were carried out in MATLAB environment using three techniques: HOG(8 x 8)+SVM, HOG(16 x 16)+SVM, and HOG(16 x 16)+ (8 x 8)+SVM (proposed system) with respect to post-processed images (image sharpening) and non-post-processed images. The following six forms of experiments were performed:

1. Non-post-processed images classification using HOG (8 x 8) +SVM technique.
2. Non-post-processed images classification using HOG (16 x 16) +SVM technique.
3. Non-post-processed images classification using a fusion of HOG (8x8) and HOG (16x16) features algorithm.
4. Post-processed images classification using HOG (8 x 8) +SVM algorithm.
5. Post-processed images classification using HOG (16 x 16) +SVM algorithm.
6. Post-processed images classification using a fusion of HOG (8x8) and HOG(16x16) features algorithm.

Table 4.1 consists of the MAD experimentation result for post-processed images.

Table 4. 1 MAD Classification Result for Post-Processed Images

Post-Processed Images (Sharpening)			
Algorithm	**Accuracy (%)**	**FRR (%) @**	
		FAR =5%	**FAR =10%**
HOG (8x8) + SVM	94.29	6.67	3.33
HOG (16x16) +SVM	90.00	19.85	9.93
HOG(8x8)+HOG(16x16)+SVM (Proposed Method)	**95.71**	**3.36**	**1.68**
Local binary pattern + Neighbourhood component analysis + Decision Tree (Kenneth *et al.*, 2021)	85%		

In comparison to HOG (8x8) +SVM and HOG (16x16) +SVM, which had accuracy of 94.29 % and 90.00%, respectively, the proposed technique attained the highest accuracy with a value of 95.71% in the post-processed images (Table 4.1). According to the BPCER values in Table 4.1, the proposed technique has the best outputs, with a BPCER of 3.36% at APCER = 5% and 1.68% at APCER = 10%. The concatenation of gradient features HOG (8x8) and HOG (16x16) derived from post-processed morphed and bona-fide images enhanced the efficiency of the proposed technique.

Figure 4.1 is the DET Curve indicating the proposed method's performance, HOG (8x8) and HOG (16x16) for post-processed images. In the Figure 4.1 SVM has an area under the curve of 1.0 when trained with the fused features and when trained with the HOG8 feature sets which made the line on the DET curve to overlap on the x and y-axis lines. However an area under the curve of 0.9989 was obtained for HOG16.

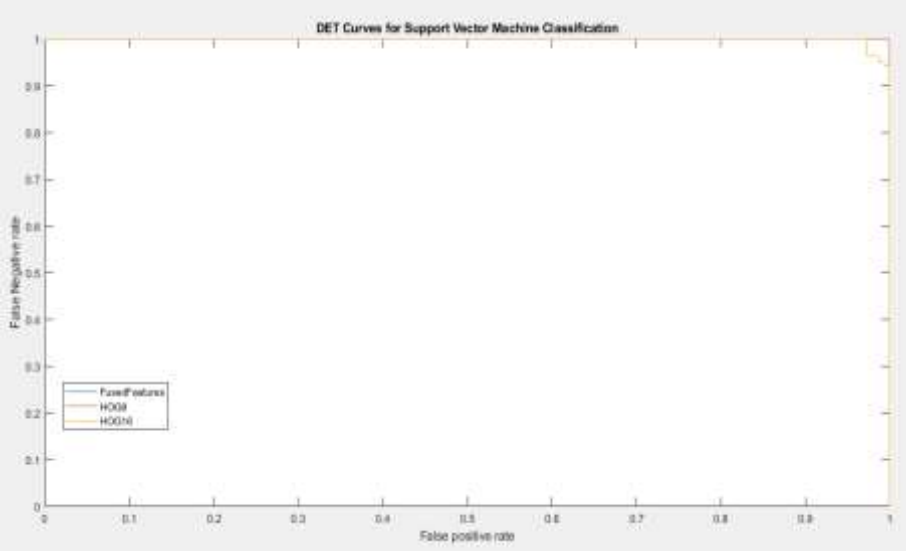

Figure 4. 1DET Curve of the proposed system, HOG (8x8) and HOG (16x16) for post-processed images

In Table 4.2, the proposed method had the best performance of 97.14% accuracy for non-post-processed images, compared to HOG (8x8) + SVM and HOG (16x16) + SVM, both of which had a 94.29% accuracy. According to the BPCER values in Table 4.2, the proposed method has the best results, with a BPCER of 1.63% at APCER = 5% and 0.82 percent at APCER = 10%. While the methods presented by Ramachandra *et al*. (2020) and Ramachandra *et al*. (2019) have BPCER of 45.76% and BPCER = 7.59% at APCER =5% and BPCER of 13.12% and BPCER = 0.86% at APCER = 10%.

Table 4. 2 MAD Classification Results for Non-Post-Processed Images

Non-Post-Processed Images			
ALGORITHM	**Accuracy (%)**	**FRR (%) @**	
		FAR =5%	**FAR =10%**
HOG (8x8) + SVM	94.29	4.93	2.47
HOG (16x16) +SVM	94.29	4.93	2.47
HOG(8x8)+HOG(16x16)+SVM (Proposed Method)	**97.14**	**1.63**	**0.82**
Steerable Textures (Ramachandra *et al*., 2020)	-	45.76	13.12
Laplacian Pyramid + LBP(Ramachandra *et al*., 2019)	-	7.59	0.86
Deep Color Residual Noise (Venkatesh *et al*., 2019b)	-	3.00	1.50
Transferable Deep-CNN (Raghavendra *et al*., 2017)		14.38	7.53

Figure 4.2 is the DET Curve indicating the proposed technique's performance, HOG (8x8) and HOG (16x16) for non-post-processed images. In the Figure 4.2 SVM has an area under the curve of 1.0 when trained with the fused features and when trained with the HOG8 feature sets which made the line on the DET curve to overlap on the x and y-axis lines. However an area under the curve of 0.9968 was obtained for HOG16.

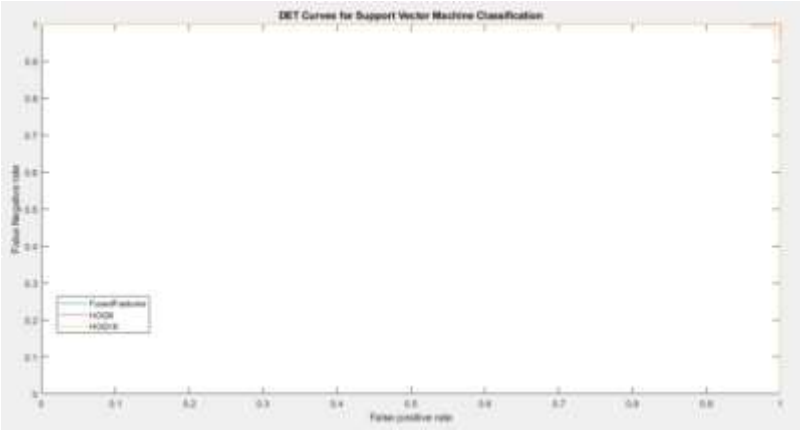

Figure 4. 2 DET Curve of the proposed system, HOG (8x8) and HOG (16x16) for non-post-processed images

In comparison to previous MAD study, this thesis was able to accomplish MAD more reliable. This is attributable to the system's ability to detect morphed images using a fusion of efficient and robust feature descriptors, even after post-processing operations have been applied to those images. Figure 4.3 shows a chart comparing the performance of seven different MAD techniques, namely HOG(8x8), HOG(16x16), proposed technique (HOG(8x8)+HOG(16x16)), steerable texture, Laplacian Pyramid + LBP, Deep colour residual noise and Transferable deep-CNN techniques. Figure 4.3 is also a visualization of the performance measures in Table 4.2.

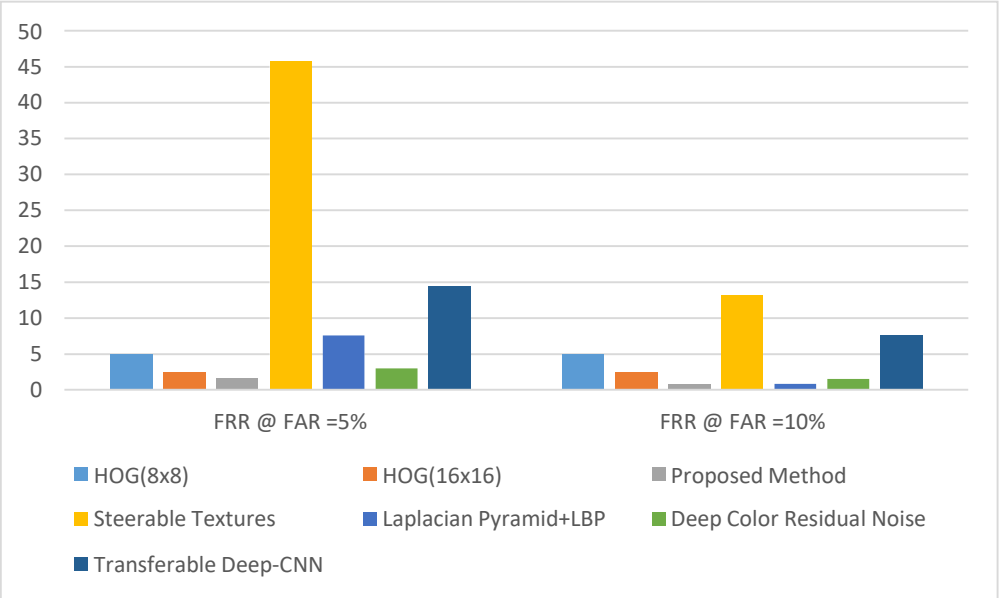

Figure 4. 3 Comparison of MAD techniques for Non-Post-Processed Images

Figure 4.4 shows a chart comparing the performance of four different MAD techniques, namely HOG(8x8), HOG(16x16), proposed technique (HOG(8x8)+HOG(16x16)) and Kenneth *et al.* (2021). Figure 4.4 is a visualization of the performance measures in Table 4.1.

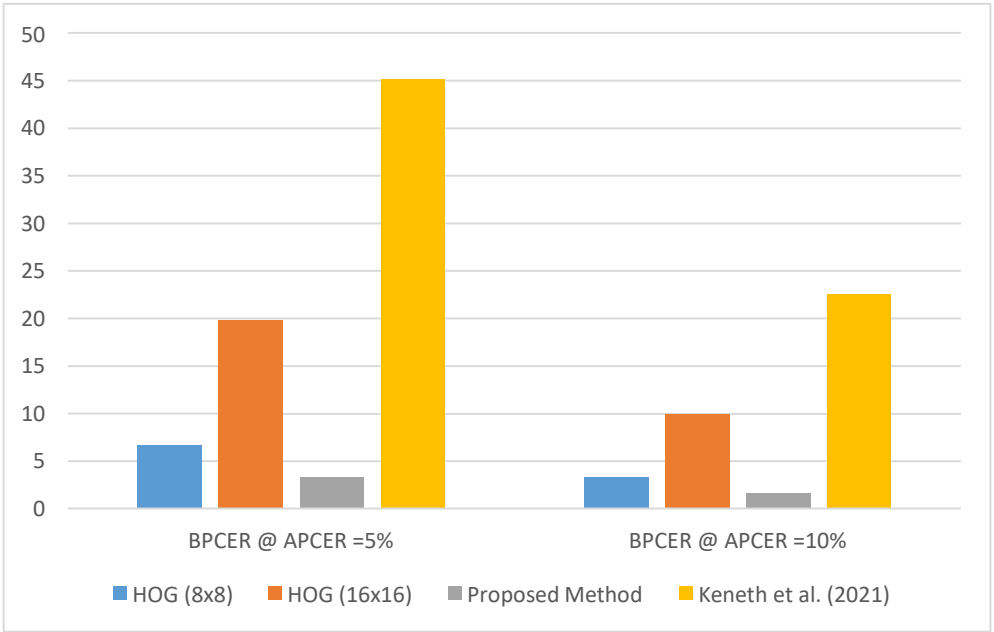

Figure 4. 4 Comparison of MAD techniques for Post-Processed Images

CHAPTER FIVE

5.0 CONCLUSION AND RECOMMENDATION

5.1 Summary

This study performed MAD even after the performing post-processing operations (sharpening) on both morphed and bona-fide images based on a combination of the HOG (8x8) and HOG (16x16) descriptor using the SVM classifier. The HOG features were extracted from the post-processed and the non-post-processed morphed and bona-fide images in this work. These extracted features were adjusted to a putatively standard scale by normalizing the features calculated on different scales. These normalized features were fused using the feature-level fusion method. The SVM classifier learned these fused features, which classified the features into two categories: morphed or bona-fide. The proposed method was compared to existing MAD techniques and single feature descriptor methods. Based on the findings, it can be inferred that the proposed system outperforms current MAD methods.

5.2 Conclusion

In conclusion, a method was proposed which performs MAD in the presence of post-processed images (morphed or bona-fide) based on averaging dimensionality reduction and summation feature-level fusion of HOG (8x8) and (16x16) gradient features using SVM. In this research work, training the model with the fused feature of HOG (8x8) and (16x16) gave a better result than using HOG (8x8) or HOG (16x16) alone.

In this thesis, the dimensionality reduction was achieved using averaging which reduced larger dimension data into the required dimension; then, the fusion was performed on the reduced dataset using the summation of features. Finally, the fused features were fed to the SVM classifier, categorising the images into morphed or bona-fide.

5.3 Contributions to Knowledge

This research made two major contributions: Firstly, a morphed image dataset and a sharpened post-processed morphed photo dataset was generated. The dataset is constructed in such a way that bias is avoided. Secondly, a dimensionality reduction and feature-level technique for detecting post-processed morphed images which are more hardened to detection was developed.

5.4 Recommendation

The morphed dataset used in this study was created in-house using morphing software that was readily accessible. Since there was no publicly accessible large database for MAD, the majority of the study was done in-house. This project resulted in a small dataset of genuine, morphed, and post-processed morphed photos. To render MAD algorithms more accurate and stable, it is suggested that a large publicly accessible morph database consisting of morphed and post-processed morphed images be developed. Since the research was performed on morphed photos created by only two morphing software, multiple morphing software should be utilized to create morphed datasets to improve MAD's reliability. Finally, traditional image post-processing operations including compression and blurring should be taken into account.

REFERENCES

123RF. (2020). Black Man Face Stock Photos and Images. *Black Man Face Stock Photos and Images*. Retrieved August 25, 2020, from https://www.123rf.com/stock-photo/black_man_face.html?sti=lo3vts77wcrg1jyzpb|

Anjana, M. V., & Sandhya, L. (2017). Implementation and Comparison of Feature Detection Methods in Image Mosaicing. *IOSR Journal of Electronics and Communication Engineering*, 6(2), 7–11. https://www.iosrjournals.org/iosr-jece/papers/Conf.17009-2017/Volume-1/2.%2007-11.pdf

Attallah, B., Serir, A., Chahir, Y., & Boudjelal, A. (2017). Histogram of gradient and binarized statistical image features of wavelet subband-based palmprint features extraction. *Journal of Electronic Imaging*, *26*(06), 1. https://doi.org/10.1117/1.JEI.26.6.063006

Azhar, M. A., & Thomas, P. A. (2019). Comparative Review of Feature Selection and Classification modeling. *2019 International Conference on Advances in Computing, Communication and Control (ICAC3)*, 1–9. https://doi.org/10.1109/ICAC347590.2019.9036816

Bay, H., Ess, A., Tuytelaars, T., & Van Gool, L. (2008). Speeded-Up Robust Features (SURF). *Computer Vision and Image Understanding*, *110*(3), 346–359. https://doi.org/10.1016/j.cviu.2007.09.014

Benkaddour, M. K., & Bounoua, A. (2017). Feature extraction and classification using deep convolutional neural networks, PCA and SVC for face recognition. *Traitement Du Signal*, *34*(1–2), 77–91. https://doi.org/10.3166/ts.34.77-91

Bharadwaj, S., Dhamecha, T. I., Vatsa, M., & Singh, R. (2013). Computationally Efficient Face Spoofing Detection with Motion Magnification. *2013 IEEE Conference on Computer Vision and Pattern Recognition Workshops*, 105–110. https://doi.org/10.1109/CVPRW.2013.23

Bhardwaj, S. K. (2014). An Algorithm for Feature Level Fusion in Multimodal Biometric System. *International Journal of Advanced Research in Computer Engineering & Technology*, *3*(10), 3499-3503. http://ijarcet.org/wp-content/uploads/IJARCET-VOL-3-ISSUE-10-3499-3503.pdf

Bonettini, N., Bondi, L., Guera, D., Mandelli, S., Bestagini, P., Tubaro, S., & Delp, E. J. (2018). Fooling PRNU-Based Detectors Through Convolutional Neural Networks. *2018 26th European Signal Processing Conference (EUSIPCO)*, 957–961. https://doi.org/10.23919/EUSIPCO.2018.8553596

Busch, C., Caillebotte, S., Seidel, U., Knopjes, F., Maltoni, D., Ferrara, M., Veldhuis, R., Spreeuwers, L., Raja, K., Raghavendra, R., Gomez-Barrero, M., & Rathgeb, C. (2019). *The Challenge of Morphing for Border Control*. 1-20. https://www.christoph-busch.de/files/Busch-Frontex-MAD-191009.pdf

Chierchia, G., Parrilli, S., Poggi, G., Verdoliva, L., & Sansone, C. (2011). PRNU-based detection of small-size image forgeries. *2011 17th International Conference on Digital Signal Processing (DSP)*, 1–6. https://doi.org/10.1109/ICDSP.2011.6004957

Chih-Wei, H., & Chih-Jen, L. (2002). A comparison of methods for multiclass support vector machines. *IEEE Transactions on Neural Networks*, *13*(2), 415–425. https://doi.org/10.1109/72.991427

Chingovska, I., Mohammadi, A., Anjos, A., & Marcel, S. (2019). Evaluation Methodologies for Biometric Presentation Attack Detection. In S. Marcel, M. S. Nixon, J. Fierrez, & N. Evans (Eds.), *Handbook of Biometric Anti-Spoofing* (pp. 457–480). Springer International Publishing. https://doi.org/10.1007/978-3-319-92627-8_20

Choras, R. (2007). Image Feature Extraction Techniques and Their Applications for CBIR and Biometrics Systems. *International Journal of Biology and Biomedical Engineering*, *1*(1), 7-16.

Crammer, K., & Singer, Y. (2001). On the Algorithmic Implementation of Multiclass Kernel-based Vector Machines. *Journal of Machine Learning Research*, 2(1), 265-295. https://dl.acm.org/doi/10.5555/944790.944813

Dalal, N., & Triggs, B. (2005). Histograms of Oriented Gradients for Human Detection. *2005 IEEE Computer Society Conference on Computer Vision and Pattern Recognition (CVPR'05)*, *1*, 886–893. https://doi.org/10.1109/CVPR.2005.177

Damer, N., Boller, V., Wainakh, Y., Boutros, F., Terhörst, P., Braun, A., & Kuijper, A. (2019). Detecting Face Morphing Attacks by Analyzing the Directed Distances of Facial Landmarks Shifts. In T. Brox, A. Bruhn, & M. Fritz (Eds.), *Pattern Recognition* (Vol. 11269, pp. 518–534). Springer International Publishing. https://doi.org/10.1007/978-3-030-12939-2_36

Damer, N., Saladie, A. M., Braun, A., & Kuijper, A. (2018a). MorGAN: Recognition Vulnerability and Attack Detectability of Face Morphing Attacks Created by Generative Adversarial Network. *2018 IEEE 9th International Conference on Biometrics Theory, Applications and Systems (BTAS)*, 1–10. https://doi.org/10.1109/BTAS.2018.8698563

Damer, N., Wainakh, Y., Henniger, O., Croll, C., Berthe, B., Braun, A., & Kuijper, A. (2018b). Deep Learning-based Face Recognition and the Robustness to Perspective Distortion. *2018 24th International Conference on Pattern Recognition (ICPR)*, 3445–3450. https://doi.org/10.1109/ICPR.2018.8545037

Debiasi, L., Rathgeb, C., Scherhag, U., Uhl, A., & Busch, C. (2018a). PRNU Variance Analysis for Morphed Face Image Detection. *2018 IEEE 9th International Conference on Biometrics Theory, Applications and Systems (BTAS)*, 1–9. https://doi.org/10.1109/BTAS.2018.8698576

Debiasi, L., Scherhag, U., Rathgeb, C., Uhl, A., & Busch, C. (2018b). PRNU-based detection of morphed face images. *2018 International Workshop on Biometrics and Forensics (IWBF)*, 1–7. https://doi.org/10.1109/IWBF.2018.8401555

Deshpande, N. T., & Ravishankar, S. (2017). Face Detection and Recognition using Viola-Jones algorithm and Fusion of PCA and ANN. *Advances in Computational Sciences and Technology*, *10*(5), 18. https://doi.org/0973-6107

Dong, W.-M., Bao, G.-B., Zhang, X.-P., & Paul, J.-C. (2012). Fast Multi-Operator Image Resizing and Evaluation. *Journal of Computer Science and Technology*, *27*(1), 121–134. https://doi.org/10.1007/s11390-012-1211-6

Ferrara, M., Franco, A., & Maltoni, D. (2016). On the Effects of Image Alterations on Face Recognition Accuracy. In T. Bourlai (Ed.), *Face Recognition Across the Imaging Spectrum* (pp. 195–222). Springer International Publishing. https://doi.org/10.1007/978-3-319-28501-6_9

Ferrara, M., Franco, A., & Maltoni, D. (2019). *Face morphing detection in the presence of printing/scanning and heterogeneous image sources*. 4(1), 1-12. https://dio.org/10.1049/bme2.12021

Ferrara, M., Franco, A., & Maltoni, D. (2014). The magic passport. *IEEE International Joint Conference on Biometrics*, 1–7. https://doi.org/10.1109/BTAS.2014.6996240

Fridrich, J. (2009). Digital Image Forensics Using Sensor Noise. *IEEE Signal Processing Magazine*, *26*(3), 1-11. https://www.semanticscholar.org/paper/Digital-Image-Forensics-Using-Sensor-Noise-Fridrich/36d15307fe3cdafe3a4a9cbb70b2b4c7bf9e5225

Fu, D., Shi, Y. Q., & Su, W. (2007). *A generalized Benford's law for JPEG coefficients and its applications in image forensics*. 65051L. https://doi.org/10.1117/12.704723

Gawande, U., Zaveri, M., & Kapur, A. (2013). A Novel Algorithm for Feature Level Fusion Using SVM Classifier for Multibiometrics-Based Person Identification. *Applied Computational Intelligence and Soft Computing*, *2013*, 1–11. https://doi.org/10.1155/2013/515918

Heikkila, M., Pietikainen, M., & Schmid, C. (2009). Description of interest regions with local binary patterns. *Pattern Recognition*, 42(3), 425-436. https://doi.org/10.1016/j.patcog.2008.08.014

Hildebrandt, M., Neubert, T., Makrushin, A., & Dittmann, J. (2017). Benchmarking face morphing forgery detection: Application of stirtrace for impact simulation of different processing steps. *2017 5th International Workshop on Biometrics and Forensics (IWBF)*, 1–6. https://doi.org/10.1109/IWBF.2017.7935087

Huang, D., Shan, C., Ardabilian, M., Wang, Y., & Chen, L. (2011). Local Binary Patterns and Its Application to Facial Image Analysis: A Survey. *IEEE Transactions on Systems, Man, and Cybernetics, Part C (Applications and Reviews)*, *41*(6), 765–781. https://doi.org/10.1109/TSMCC.2011.2118750

İLeri, S. C., KarabiNa, A., & Kiliç, E. (2018). Comparison of Different Normalization Techniques on Speakers' Gender Detection. *Journal of Applied Sciences of*

Mehmet Akif Ersoy University, *2*(2), 12. https://doi.org/10.31200/makuubd.410625

Jassim, S., & Asaad, A. (2018). Automatic Detection of Image Morphing by Topology-based Analysis. *2018 26th European Signal Processing Conference (EUSIPCO)*, 1007–1011. https://doi.org/10.23919/EUSIPCO.2018.8553317

Jensen, O. H. (2008). *Implementing the Viola-Jones Face Detection Algorithm* (No. 87-643-0008–0; p. 36). IMM·DTU.

Jeyashree, N. P., & Deepak, A. (2018). Detection of Retinal Disease by Local Binary Pattern. *International Journal of Pure and Applied Mathematics*, *119*(15), 10.https://doi.org/ 10.1007/978-981-13-5802-9_91

Kalapatapu, P., Goli, S., Arthum, P., & Malapati, A. (2016). A Study on Feature Selection and Classification Techniques of Indian Music. *Procedia Computer Science*, *98*, 125–131. https://doi.org/10.1016/j.procs.2016.09.020

Kannala, J., & Rahtu, E. (2012). BSIF: Binarized Statistical Image Features. *21st International Conference on Pattern Recognition (ICPR 2012)* 1(4), 1363-1366.

Kenneth, O. M., Sulaimon, A. B., Opeyemi, A. A., & Mohammed, A. D. (2021). Face Morphing Attack Detection in the Presence of Post-processed Image Sources Using Neighborhood Component Analysis and Decision Tree Classifier. *Misra S., Muhammad-Bello B. (Eds) Information and Communication Technology and Applications. ICTA 2020., 1350*, 340–354. https://doi.org/10.1007/978-3-030-69143-1_27

Kolbaşi, A., & Ünsal, P. A. (2015). A Comparison of the Outlier Detecting Methods: An Application on Turkish Foreign Trade Data. *Journal of Mathematics and Statistical Science*, *5*, 213–234.

Korshunova, I., Shi, W., Dambre, J., & Theis, L. (2017). Fast Face-swap Using Convolutional Neural Networks. *IEEE International Conference on Computer Vision (ICCV)*, 3697-3705. http://doi.org/ 10.1109/ICCV.2017.397

Kraetzer, C., Makrushin, A., Neubert, T., Hildebrandt, M., & Dittmann, J. (2017). Modeling Attacks on Photo-ID Documents and Applying Media Forensics for the Detection of Facial Morphing. *Proceedings of the 5th ACM Workshop on Information Hiding and Multimedia Security - IHMMSec '17*, 21–32. https://doi.org/10.1145/3082031.3083244

Kramer, R. S. S., Mireku, M. O., Flack, T. R., & Ritchie, K. L. (2019). Face morphing attacks: Investigating detection with humans and computers. *Cognitive Research: Principles and Implications*, *4*(1), 28. https://doi.org/10.1186/s41235-019-0181-4

Kumar, B. S., Verma, K., & S. Thoke, A. (2015). Investigations on Impact of Feature Normalization Techniques on Classifier's Performance in Breast Tumor Classification. *International Journal of Computer Applications*, *116*(19), 11–15. https://doi.org/10.5120/20443-2793

Kumar, G., & Bhatia, P. K. (2014). A Detailed Review of Feature Extraction in Image Processing Systems. *2014 Fourth International Conference on Advanced Computing & Communication Technologies*, 5–12. https://doi.org/10.1109/ACCT.2014.74

Kumar, T., & Verma, K. (2010). A Theory Based on Conversion of RGB image to Gray image. *International Journal of Computer Applications*, *7*(2), 5–12. https://doi.org/10.5120/1140-1493

Lin, E. O. W., Pan, F., & Moscheni, F. (2003). A No-Reference Quality Metric For Measuring Image Blur. *Seventh International Symposium on Signal Processing and Its Applications, 1(1),* 469-472. https://doi.org/ 10.1109/ISSPA.2003.1224741

Liu, Z., Luo, P., Wang, X., & Tang, X. (2015). Deep Learning Face Attributes in the Wild. *2015 IEEE International Conference on Computer Vision (ICCV)*, 3730–3738. https://doi.org/10.1109/ICCV.2015.425

Lowe, D. G. (1999). Object recognition from local scale-invariant features. *Proceedings of the Seventh IEEE International Conference on Computer Vision*, 1150–1157 vol.2. https://doi.org/10.1109/ICCV.1999.790410

Makrushin, A., Kraetzer, C., Neubert, T., & Dittmann, J. (2018). Generalized Benford's Law for Blind Detection of Morphed Face Images. *Proceedings of the 6th ACM Workshop on Information Hiding and Multimedia Security*, 49–54. https://doi.org/10.1145/3206004.3206018

Makrushin, A., Neubert, T., & Dittmann, J. (2017). Automatic Generation and Detection of Visually Faultless Facial Morphs: *Proceedings of the 12th International Joint Conference on Computer Vision, Imaging and Computer Graphics Theory and Applications*, 39–50. https://doi.org/10.5220/0006131100390050

Makrushin, A., & Wolf, A. (2018). An Overview of Recent Advances in Assessing and Mitigating the Face Morphing Attack. *2018 26th European Signal Processing Conference (EUSIPCO)*, 1017–1021. https://doi.org/10.23919/EUSIPCO.2018.8553599

Malini, Manjunatha., & Patil, M. (2018). Interpolation Techniques in Image Resampling. *International Journal of Engineering & Technology*, *7*(3.34), 567. https://doi.org/10.14419/ijet.v7i3.34.19383

Meyer, D., Leisch, F., & Hornik, K. (2003). The support vector machine under test. *Neurocomputing*, *55*(1–2), 169–186. https://doi.org/10.1016/S0925-2312(03)00431-4

Mills, P. (2011). Efficient statistical classification of satellite measurements. *International Journal of Remote Sensing*, *32*(21), 6109–6132. https://doi.org/10.1080/01431161.2010.507795

Mislav, G., Kresimir, D., Sonja, G., & Bozidar, K. (2021, February 2). Surveillance Cameras Face Database. *Multimedia Tools and Applications Journal, 55(3), 863-879*. https://www.scface.org/

Mohammadi, A., Bhattacharjee, S., & Marcel, S. (2018). Deeply vulnerable: A study of the robustness of face recognition to presentation attacks. *IET Biometrics, 7*(1), 15–26. https://doi.org/10.1049/iet-bmt.2017.0079

Nanni, L., Lumini, A., & Brahnam, S. (2010). Local binary patterns variants as texture descriptors for medical image analysis. *Artificial Intelligence in Medicine*, 49(2), 117-125. https://doi.org/10.1016/j.artmed.2010.02.006

Neubert, T., Kraetzer, C., & Dittmann, J. (2019). A Face Morphing Detection Concept with a Frequency and a Spatial Domain Feature Space for Images on eMRTD. *Proceedings of the ACM Workshop on Information Hiding and Multimedia Security*, 95–100. https://doi.org/10.1145/3335203.3335721

Olivier, R., & Hanqiang, C. (2012). Nearest Neighbor Value Interpolation. *International Journal of Advanced Computer Science and Applications*, *3*(4), 1-6. https://doi.org/10.14569/IJACSA.2012.030405

Ortega-Delcampo, D., Conde, C., Palacios-Alonso, D., & Cabello, E. (2020). Border Control Morphing Attack Detection with a Convolutional Neural Network De-morphing Approach. *IEEE Access*, 8, 92301–92313. https://doi.org/10.1109/ACCESS.2020.2994112

Panchal, P. M., Panchal, S. R., & Shah, S. K. (2013). A Comparison of SIFT and SURF. *International Journal of Innovative Research in Computer and Communication Engineering*, *1*(2), 323-327.

Parsania, Mr. P. S., & Virparia, Dr. P. V. (2016). A Comparative Analysis of Image Interpolation Algorithms. *IJARCCE*, *5*(1), 29–34. https://doi.org/10.17148/IJARCCE.2016.5107

Patel, A. (2015). Image Morphing Algorithm: A Survey. *International Journal of Computer Application*, *5*(3), 156-160.

Peng, F., Zhang, L.-B., & Long, M. (2019). FD-GAN: Face De-Morphing Generative Adversarial Network for Restoring Accomplice's Facial Image. *IEEE Access*, *7*, 75122–75131. https://doi.org/10.1109/ACCESS.2019.2920713

Raghavendra, R., Raja, K. B., & Busch, C. (2016). Detecting morphed face images. *2016 IEEE 8th International Conference on Biometrics Theory, Applications and Systems (BTAS)*, 1–7. https://doi.org/10.1109/BTAS.2016.7791169

Raghavendra, R., Raja, K. B., Venkatesh, S., & Busch, C. (2017). Transferable Deep-CNN Features for Detecting Digital and Print-Scanned Morphed Face Images. *2017 IEEE Conference on Computer Vision and Pattern Recognition Workshops (CVPRW)*, 1822–1830. https://doi.org/10.1109/CVPRW.2017.228

Ramachandra, R., Venkatesh, S., Raja, K., & Busch, C. (2020). Detecting Face Morphing Attacks with Collaborative Representation of Steerable Features. In B. B. Chaudhuri, M. Nakagawa, P. Khanna, & S. Kumar (Eds.), *Proceedings of 3rd International Conference on Computer Vision and Image Processing* (Vol. 1022, pp. 255–265). Springer Singapore. https://doi.org/10.1007/978-981-32-9088-4_22

Ramachandra, R., Venkatesh, S., Raja, K., & Busch, C. (2019). Towards making Morphing Attack Detection robust using hybrid Scale-Space Colour Texture Features. *2019 IEEE 5th International Conference on Identity, Security, and Behavior Analysis (ISBA)*, 1–8. https://doi.org/10.1109/ISBA.2019.8778488

Robertson, D. J., Mungall, A., Watson, D. G., Wade, K. A., Nightingale, S. J., & Butler, S. (2018). Detecting morphed passport photos: A training and individual differences approach. *Cognitive Research: Principles and Implications*, *3*(1), 27. https://doi.org/10.1186/s41235-018-0113-8

Saravanan, C. (2010). Color Image to Grayscale Image Conversion. *2010 Second International Conference on Computer Engineering and Applications*, 196–199. https://doi.org/10.1109/ICCEA.2010.192

Scherhag, U., Budhrani, D., Gomez-Barrero, M., & Busch, C. (2018a). Detecting Morphed Face Images Using Facial Landmarks. In A. Mansouri, A. El Moataz, F. Nouboud, & D. Mammass (Eds.), *Image and Signal Processing* (Vol. 10884, pp. 444–452). Springer International Publishing. https://doi.org/10.1007/978-3-319-94211-7_48

Scherhag, U., Debiasi, L., Rathgeb, C., Busch, C., & Uhl, A. (2019a). Detection of Face Morphing Attacks Based on PRNU Analysis. *IEEE Transactions on Biometrics, Behavior, and Identity Science*, *1*(4), 302–317. https://doi.org/10.1109/TBIOM.2019.2942395

Scherhag, U., Nautsch, A., Rathgeb, C., Gomez-Barrero, M., Veldhuis, R. N. J., Spreeuwers, L., Schils, M., Maltoni, D., Grother, P., Marcel, S., Breithaupt, R., Ramachandra, R., & Busch, C. (2017). Biometric Systems under Morphing Attacks: Assessment of Morphing Techniques and Vulnerability Reporting. *2017 International Conference of the Biometrics Special Interest Group (BIOSIG)*, 1–7. https://doi.org/10.23919/BIOSIG.2017.8053499

Scherhag, U., Rathgeb, C., & Busch, C. (2018b). Detection of morphed faces from single images: A multi-algorithm fusion approach. *Proceedings of the 2018 2nd International Conference on Biometric Engineering and Applications, 6-12*. https://doi.org/10.1145/3230820.3230822

Scherhag, U., Rathgeb, C., & Busch, C. (2018c). Towards Detection of Morphed Face Images in Electronic Travel Documents. *2018 13th IAPR International Workshop on Document Analysis Systems (DAS)*, 187–192. https://doi.org/10.1109/DAS.2018.11

Scherhag, U., Rathgeb, C., Merkle, J., Breithaupt, R., & Busch, C. (2019b). Face Recognition Systems Under Morphing Attacks: A Survey. *IEEE Access*, *7*, 23012–23026. https://doi.org/10.1109/ACCESS.2019.2899367

Scherhag, U., Rathgeb, C., Merkle, J., & Busch, C. (2020). Deep Face Representations for Differential Morphing Attack Detection. *IEEE Transactions on Information Forensics and Security, 15, 3625-3639.* https://doi.org/10.1109/TIFS.2020.2994750

Seibold, C., Samek, W., Hilsmann, A., & Eisert, P. (2017). Detection of Face Morphing Attacks by Deep Learning. In C. Kraetzer, Y.-Q. Shi, J. Dittmann, & H. J. Kim (Eds.), *Digital Forensics and Watermarking* (Vol. 10431, pp. 107–120). Springer International Publishing. https://doi.org/10.1007/978-3-319-64185-0_9

Seibold, C., Samek, W., Hilsmann, A., & Eisert, P. (2018). Accurate and Robust Neural Networks for Security Related Applications Exampled by Face Morphing Attacks. *Journal of Information Security and Applications*, 53, 1-14. https://doi.org/10.1016/j.jisa.2020.102526

Seibold, C., Samek, W., Hilsmann, A., & Eisert, P. (2020). Accurate and robust neural networks for face morphing attack detection. *Journal of Information Security and Applications*, *53*, 102526. https://doi.org/10.1016/j.jisa.2020.102526

Sembiring, R. W., Zain, J. M., & Embong, A. (2011). Dimension Reduction of Health Data Clustering. *International Journal on New Computer Architectures and Their Applications (IJNCAA),*1(3), 1041-1050.

Shalabi, L. A., Shaaban, Z., & Kasasbeh, B. (2006). Data Mining: A Preprocessing Engine. *Journal of Computer Science*, *2*(9), 735–739. https://doi.org/10.3844/jcssp.2006.735.739

Shinozuka, M., & Mansouri, B. (2009). Synthetic aperture radar and remote sensing technologies for structural health monitoring of civil infrastructure systems. In *Structural Health Monitoring of Civil Infrastructure Systems* (pp. 113–151). Elsevier. https://doi.org/10.1533/9781845696825.1.114

Simoncelli, E. P., & Freeman, W. T. (1995). The steerable pyramid: A flexible architecture for multi-scale derivative computation. *Proceedings., International Conference on Image Processing*, *3*, 444–447. https://doi.org/10.1109/ICIP.1995.537667

Singh, J. M., Ramachandra, R., Raja, K. B., & Busch, C. (2019). Robust Morph-Detection at Automated Border Control Gate using Deep Decomposed 3D Shape and Diffuse Reflectance. *ArXiv:1912.01372 [Cs]*. http://arxiv.org/abs/1912.01372

Song, K.-C., Yan, Y.-H., Chen, W.-H., & Zhang, X. (2013). Research and Perspective on Local Binary Pattern. *Acta Automatica Sinica*, *39*(6), 730–744. https://doi.org/10.1016/S1874-1029(13)60051-8

Sopharak, A., Dailey, M. N., Uyyanonvara, B., Barman, S., Williamson, T., Nwe, K. T., & Moe, Y. A. (2010). Machine learning approach to automatic exudate detection in retinal images from diabetic patients. *Journal of Modern Optics*, *57*(2), 124–135. https://doi.org/10.1080/09500340903118517

Spreeuwers, L., Schils, M., & Veldhuis, R. (2018). Towards Robust Evaluation of Face Morphing Detection. *2018 26th European Signal Processing Conference (EUSIPCO)*, 1027–1031. https://doi.org/10.23919/EUSIPCO.2018.8553018

Suard, F., Rakotomamonjy, A., Bensrhair, A., & Broggi, A. (2006). Pedestrian Detection using Infrared images and Histograms of Oriented Gradients. *2006 IEEE*

Intelligent Vehicles Symposium, 206–212. https://doi.org/10.1109/IVS.2006.1689629

Sudha, D., & Ramakrishna, M. (2017). Comparative Study of Features Fusion Techniques. *2017 International Conference on Recent Advances in Electronics and Communication Technology (ICRAECT)*, 235–239. https://doi.org/10.1109/ICRAECT.2017.39

Surasak, T., Takahiro, I., Cheng, C. H., Wang, C. E., & Sheng, P. Y. (2018). Histogram of oriented gradients for human detection in video. *Proceedings of 2018 5th International Conference on Business and Industrial Research: Smart Technology for Next Generation of Information, Engineering, Business and Social Science, ICBIR 2018*, 172–176. https://doi.org/10.1109/ICBIR.2018.8391187

Tolosana, R., Gomez-Barrero, M., Busch, C., & Ortega-Garcia, J. (2020). Biometric Presentation Attack Detection: Beyond the Visible Spectrum. *IEEE Transactions on Information Forensics and Security*, *15*, 1261–1275. https://doi.org/10.1109/TIFS.2019.2934867

Venkatesh, S., Ramachandra, R., Raja, K., & Busch, C. (2020). Single Image Face Morphing Attack Detection Using Ensemble of Features. *2020 IEEE 23rd International Conference on Information Fusion (FUSION)*, 1–6. https://doi.org/10.23919/FUSION45008.2020.9190629

Venkatesh, S., Ramachandra, R., Raja, K., Spreeuwers, L., Veldhuis, R., & Busch, C. (2019a). *Detecting Morphed Face Attacks Using Residual Noise from Deep Multi-scale Context Aggregation Network*. 269-278. https://doi.org/10.1109/WACV45572.2020.9093488

Venkatesh, S., Ramachandra, R., Raja, K., Spreeuwers, L., Veldhuis, R., & Busch, C. (2019b). Morphed Face Detection Based on Deep Color Residual Noise. *2019 Ninth International Conference on Image Processing Theory, Tools and Applications (IPTA)*, 1–6. https://doi.org/10.1109/IPTA.2019.8936088

Viola, P., & Jones, M. (2001). Rapid object detection using a boosted cascade of simple features. *Proceedings of the 2001 IEEE Computer Society Conference on Computer Vision and Pattern Recognition. CVPR 2001*, *1*, I 511-I–518. https://doi.org/10.1109/CVPR.2001.990517

Wandzik, L., Garcia, R. V., Kaeding, G., & Chen, X. (2017). CNNs Under Attack: On the Vulnerability of Deep Neural Networks Based Face Recognition to Image Morphing. In C. Kraetzer, Y.-Q. Shi, J. Dittmann, & H. J. Kim (Eds.), *Digital Forensics and Watermarking* (Vol. 10431, pp. 121–135). Springer International Publishing. https://doi.org/10.1007/978-3-319-64185-0_10

Wandzik, L., Kaeding, G., & Garcia, R. V. (2018). Morphing Detection Using a General-Purpose Face Recognition System. *2018 26th European Signal Processing Conference (EUSIPCO)*, 1012–1016. https://doi.org/10.23919/EUSIPCO.2018.8553375

Wang, Y.-Q. (2014). An Analysis of the Viola-Jones Face Detection Algorithm. *Image Processing On Line*, *4*, 128–148. https://doi.org/10.5201/ipol.2014.104

Weng, Y., Wang, L., Li, X., Chai, M., & Zhou, K. (2013). Hair Interpolation for Portrait Morphing. *Computer Graphics Forum*, *32*(7), 79–84. https://doi.org/10.1111/cgf.12214

Wolberg, G. (1998). Image morphing: A survey. *The Visual Computer*, *14*(8–9), 360–372. https://doi.org/10.1007/s003710050148

Yale Face Database. (2020, November 11). [Computer Vision]. *Yale Face Database*. Retrieved August 25, 2020, from http://vision.ucsd.edu/content/yale-face-database

Yang, W., Wang, K., & Zuo, W. (2012). Neighborhood Component Feature Selection for High-Dimensional Data. *Journal of Computers*, *7*(1), 161–168. https://doi.org/10.4304/jcp.7.1.161-168

Yang, Z., & Ai, H. (2005). Demographic Classification with Local Binary Patterns. In: Lee SW., Li S.Z. (eds) Advances in Biometrics. ICB 2007. Lecture Notes in Computer Science, *Springer, Berlin, Heidelberg*, 4642. https://doi.org/10.1007/978-3-540-74549-5_49

Zhang, L.-B., Peng, F., & Long, M. (2018). Face Morphing Detection Using Fourier Spectrum of Sensor Pattern Noise. *2018 IEEE International Conference on Multimedia and Expo (ICME)*, 1–6. https://doi.org/10.1109/ICME.2018.8486607

Zhou Wang, Sheikh, H. R., & Bovik, A. C. (2002). No-reference perceptual quality assessment of JPEG compressed images. *Proceedings. International Conference on Image Processing*, *1*, I-477-I–480. https://doi.org/10.1109/ICIP.2002.1038064

Zhu, Z., Zhang, G., & Li, H. (2018). SURF feature extraction algorithm based on visual saliency improvement. *International Journal of Engineering and Applied Sciences*, 5(3), 13-17. Retrieved from https://www.neliti.com/publications/257267/surf-feature-extraction-algorithm-based-on-visual-saliency-improvement

APPENDIX A

Source Code For Dimensionality Reduction And Feature-Level Fusion

```
[rows_16, columns_16]  = size(enhancedHOG16);  % get the size of the HOG16 dimension matrix

[rows_8, columns_8]    = size(enhancedHOG8);      % get the size of the HOG8 dimension matrix

%assign number of columns for large and small matrix to m and n respectively

n = columns_16;

m = columns_8;

%Floor value of number of columns of HOG8 matrix divided by number of columns of HOG16 matrix

m1=floor(m/n);        %The greatest integer that is less than or equal to m/n

m2=m-(m1*n)+m1;

 %looping through rows of large matrix

for i = 1:rows_16

   P =enhancedHOG8(i, :);

   Q1=mean(P(1:m2));                    %Average of first selected columns

   for t=m2+1:m1:m                      %Loop starting from point m2, incremented by m1 and ends at m

      Q1=[Q1;mean(P(t:t+m1-1))];     %concatenate average of first selected sets of columns with the remaining columns average

   end

      HOG8merged(i,:)    = (Q1);    %Merge each rows

end

mergedHOG8 =(HOG8merged);
```

```
%Feature Fusion of HOG8 and HOG16

HOG8ANDHOG16       = mergedHOG8 + enhancedHOG16;

ehanced_fused_feature3 =HOG8ANDHOG16;

enhanced_fused_feature4 =[enhancedHOG16 HOG8ANDHOG16];

%Store  file to path

base_path = 'C:\Users\PC\Documents\resized images';

myFiles = fullfile(base_path,sprintf('enhanced_fused_feature3.csv'));

csvwrite(myFiles,ehanced_fused_feature3)
```

APPENDIX B

Source Code For Classification

```
%80:20

%Training Dataset

Ax_train = Ax_train(1:280,:);

Bx_train = Bx_train(1:280,:);

Dx_train = Dx_train(1:280,:);

y_train = y_train(1:280,:);

%Testing  Dataset

Ax_test = Ex_test(1:70,:);

Bx_test = Bx_test(1:70,:);

Dx_test = Dx_test(1:70,:);

y_test = y_test(1:70,:);

%% Classification

Amdl = fitcsvm(Ax_train,y_train);

Bmdl = fitcsvm(Bx_train,y_train);

Dmdl = fitcsvm(Dx_train,y_train);

%% Accuracy

Aacc= sum(predict(Amdl,Ax_test)== y_test)/length(y_test)*100

Bacc= sum(predict(Bmdl,Bx_test)== y_test)/length(y_test)*100

Dacc= sum(predict(Dmdl,Dx_test)== y_test)/length(y_test)*100

Ate = predict(Amdl,Ax_test); Bte = predict(Bmdl,Bx_test); Dte =
predict(Dmdl,Dx_test);
```

```
ACon = confusionmat(y_test,Ate); BCon = confusionmat(y_test,Bte); DCon = confusionmat(y_test,Dte);

Acon1 = ACon(1:1,1:1); Bcon1 = BCon(1:1,1:1); Dcon1 = DCon(1:1,1:1);

Acon2 = ACon(1:1,2:2); Bcon2 = BCon(1:1,2:2); Dcon2 = DCon(1:1,2:2);

Acon3 = ACon(2:2,1:1); Bcon3 = BCon(2:2,1:1); Dcon3 = DCon(2:2,1:1);

Acon4 = ACon(2:2,2:2); Bcon4 = BCon(2:2,2:2); Dcon4 = DCon(2:2,2:2);

Afnr = Acon3/(Acon1+Acon3); Bfnr = Bcon3/(Bcon1+Bcon3); Dfnr = Dcon3/(Dcon1+Dcon3);

Afpr = Acon2/(Acon4+Acon2); Bfpr = Bcon2/(Bcon4+Bcon2); Dfpr = Dcon2/(Dcon4+Dcon2);

 Ak    = Afnr * Afpr;  Bk    = Bfnr * Bfpr;  Dk    = Dfnr * Dfpr;

Afnr5 = Ak/0.05;  Bfnr5 = Bk/0.05;   Dfnr5 = Dk/0.05;

Afnr10= Ak/0.10; Bfnr10= Bk/0.10;  Dfnr10= Dk/0.10;

%ROC Curve

AmdlSVM     = fitPosterior(Amdl); BmdlSVM = fitPosterior(Bmdl); DmdlSVM = fitPosterior(Dmdl);

[~,Ascore]      = resubPredict(AmdlSVM); [~,Bscore] = resubPredict(BmdlSVM);
[~,Dscore]      = resubPredict(DmdlSVM);

[AX,AY,AT,AAUC] = perfcurve(y_train,Ascore(:,1),1, 'YCrit','fnr');

[BX,BY,BT,BAUC] = perfcurve(y_train,Bscore(:,1),1, 'YCrit','fnr');

[DX,DY,DT,DAUC] = perfcurve(y_train,Dscore(:,1),1, 'YCrit','fnr');

 plot(AX,AY)

hold on

plot(BX,BY)

plot(DX,DY)
```

```
legend('FusedFeatures','HOG8','HOG16','Location','Best')

xlabel('False positive rate'); ylabel('False Negative rate');

title('DET Curves for Support Vector Machine Classification')

hold off
```